Chapter 12
Microscale Field-Flow Fractionation: Theory and Practice

Himanshu J. Sant and Bruce K. Gale

State of Utah Center of Excellence for Biomedical Microfluidics,
Department of Bioengineering and Department of Mechanical Engineering,
University of Utah, 50 S. Central Campus Drive, Rm. 2110,
Salt Lake City UT 84112, USA

1. Introduction

The last decade has seen exponential growth in the development of lab-on-a-chip or micro-total-analysis system (μ-TAS) components to create better, faster, and cheaper chemical and biological analysis platforms [1]. Lab-on-a-chip type analysis systems typically include a separation-based sample preparation unit to achieve this objective or to prepare the sample for further interrogation using orthogonal techniques. Researchers have employed a host of sample preparation techniques based on electrophoresis [2, 3], ultrasound [4, 5], flow [6, 7], mechanical ratchets [8, 9], electrokinetics [10, 11], packed bed systems [12], membranes [13] magnetics [14, 15], temperature [16], optics [17], dielectrophoresis [18, 19], and so forth. Microscale field-flow fractionation (FFF) techniques have been an integral part of these efforts. Most of these techniques are simply miniaturized versions of conventional macroscale units with the rationale being that the reduction in physical size of the instrument results in smaller sample volumes and faster analysis times. While, many of these systems work well when miniaturized, this approach proves inadequate for systems that do not scale well. FFF, at least for many subtypes, has been shown to scale very well and FFF meets many of the design challenges for a successful separation module in a μ-TAS including (a) ease of manufacturing, (b) low power, (c) wide range of sample type and size, (d) integration to fluidic

components, and (e) material compatibility. Thus, FFF is potentially an important solution to many problems in microfluidic system design.

Field-flow fractionation clearly improves when miniaturized due to the reduction in sample and carrier volumes, analysis times, and more notably an increase in the separation resolution (at least for the electrical and thermal subtypes). Other advantages of miniaturized FFF can include the following: parallel processing with multiple separation channels, batch fabrication with reduced costs, high quality manufacturing, and potentially disposable systems. Additionally, the possibility of on-chip sample injection, detection, and signal processing favors the microfabrication of FFF systems.

Several demonstrations of the effectiveness of FFF systems on the microscale have been made and will be reviewed in the work. Techniques that are often lumped in with FFF include split flow thin cell (SPLITT) fractionation and hydrodynamic chromatography. These related techniques have also been miniaturized and will be discussed later in this work.

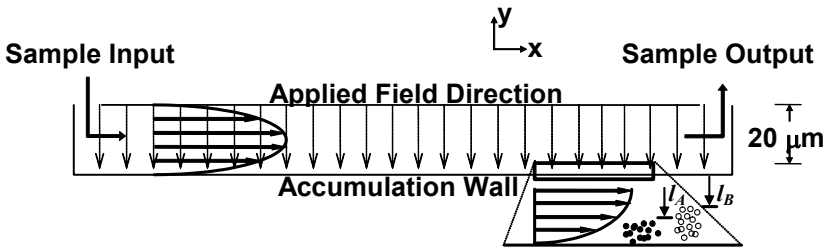

Fig. 1. FFF operational principle with two parallel plate type channel walls, laminar flow profile with transverse field direction and location of particle clouds near accumulation wall. The particle clouds depicted by closed circles and open circles in inset figure are particle cloud A with average thickness l_A, and particle cloud B with average thickness l_B, respectively

2. Background and Theory

FFF is a versatile separation technique that relies on the dual effect of the flow behavior and field distribution in a thin, open channel. FFF channels typically consist of a thin spacer enclosed by two parallel plates, modified to impart the external field as shown in Fig. 1. Flow in the channel is laminar resulting in a parabolic fluid velocity profile with differential velocity zones across the height of the channel. The versatility of FFF stems from the numerous types of fields and operating modes that can be employed to separate a wide range of sample types. Researchers over the years have developed different types of FFF systems differentiated primarily by the

type of the field employed. Electrical, thermal, magnetic, sedimentation, flow, and dielectrophoretic fields are all commonly used in FFF. In FFF the field is applied perpendicular to the flow of the carrier. Like in chromatography, an impulse injection of sample is made into a continuously flowing carrier solution. Under the influence of the applied field and possibly other hydrodynamic or gravitational forces, the injected sample migrates to an equilibrium position between the two walls of the channel, as shown in Fig. 1. The location of the equilibrium depends on the operating mode of the FFF channel, as will be discussed shortly. Sample particles then travel down the channel at the velocity associated with the flow at the equilibrium distance from the wall. Selectivity in FFF separations is determined by the system's ability to differentially retain the samples based on their physiochemical properties. FFF operational parameters like field and flow rate can be varied to allow the user to tune resolution and analysis times for a given set of sample particles. FFF channels are also naturally gentle and can be used with delicate samples such as cells and liposomes since there is no stationary phase and the shear rates are low. In addition, a single channel can be used to separate a large range of sample sizes, thus enhancing the utility of FFF instruments when compared to many chromatography techniques.

2.1. FFF Operating Modes and SPLITT Fractionation

FFF can be classified into five broad modes of operation based on the separation mechanism: (a) normal, (b) steric, (c) focusing, (d) cyclical, and (e) zero-field or hydrodynamic FFF.

In normal or classical FFF, the sample particles are forced towards the accumulation wall by the applied field. At the accumulation wall, diffusive forces associated with Brownian motion cause particles to move away from the accumulation wall. At equilibrium, the field-induced migrative forces and diffusive forces balance each other and generate an exponential concentration profile of the particle cloud. The average distance l of the particle cloud from the wall depends on the extent of interaction between the particles and the field and determines the average rate of travel for a particle down the length of the separation channel. For a mixture of particles "A" and "B" in a FFF channel as shown in Fig. 1, if $l_A < l_B$, then the "B" particles will spend relatively more time in the high velocity zone and move faster down the length of the channel compared to the "A" particles. Thus retention and separation can be generated by manipulating the average distance a particle spends away from the wall. For particles with similar mobilities, larger particles tend to be forced closer to the wall due to

their slower diffusion and so smaller particles typically elute from the FFF channel first.

The limit to normal FFF occurs when high field strengths force the sample particles to contact the wall. The distance particles are away from the wall is then controlled by the diameter of the particle or steric effects, and this is referred to as the steric mode of FFF. In steric mode, larger particles protrude farther into the flow stream than do smaller particles and thus larger particles elute first. For microscale systems that generate relatively high fields, the on-set of steric FFF is an important factor in microscale system evaluation. In steric FFF, the elution sequence is reversed in comparison to normal FFF with larger particles eluting earlier.

Another FFF mode related to steric FFF is focusing FFF or hyperlayer FFF. This mode is realized by controlling the location of the equilibrium concentration distribution inside the channel. In the case of focusing FFF, a Gaussian-type concentration profile is generated within the separation channel by using a balance of dispersive flux and migrative flux. Retention can be induced by differentially controlling the lift for different sets of particles away from the accumulation wall. Since lift is generally more significant for larger particles, they tend to move away from the accumulation wall and towards the center of the channel, which causes them to elute before smaller particles. Thus elution patterns are similar to those for steric mode of FFF and it can often be challenging to determine which mode is in operation using only experimental results. Generally, higher carrier velocities are associated with this mode and that can result in shorter elution times.

A recently developed microscale FFF mode involves the use of cyclical fields instead of a steady, uniform field. In this case, particles move either back and forth between the walls or oscillate against one wall of the channel. The retention time for the particle is determined by whether the particle spends more time in the fast flow lines or in the slower flow areas. The amount of time spent in the different flow areas can be tuned by adjusting the field strength and the frequency of the applied field. Cyclical methods have primarily been demonstrated with electrical systems and have the advantage that retention is dependent only upon the susceptibility of the particle to the applied field. Equilibrium processes are not involved and diffusion processes are essentially eliminated from the retention process, so very high speed separations can be generated.

Another technique very closely related to FFF is the SPLITT technique, which generates a continuous separation process. SPLITT has two separate inlets for the sample mixture and a carrier and two outlets for the bifurcated/separated samples. The carrier stream compresses the sample particles against one wall and the field perpendicular to the flow drives sample particles

with some minimum interaction across the carrier stream interface where they elute from the opposite outlet. Particles that do not exhibit this minimum interaction with the field continue in the original sample stream and elute from the outlet on the same side as the sample inlet port. SPLITT typically induces very fast fractionation and can be used in serial and parallel fashion to separate complex mixtures with high resolution and high throughput.

A technique called hydrodynamic chromatography is also related to FFF and is generated when the field in the FFF channel is zero such that there is no transverse flux of the particles due to the field and particles are dispersed randomly in the channel. When the particle sizes are comparable to the channel thickness, larger particles will be located in the higher velocity zones as they can not approach as close to the channel walls as smaller particles might due to their large size. In contrast, smaller particles can, on average, approach closer to the channel walls and spend more time in slower velocity zones. This zero-field separation mode has an elution sequence similar to steric FFF. Typically the size selectivity of this technique is poor but can prove to be an efficient tool to separate larger macromolecules.

2.2. FFF Retention Theory

In general, the theory behind FFF systems is well developed [20–22] and in principle the theory can be applied to all the FFF subtypes, including microscale FFF systems. The FFF channel, as shown in Fig. 1, is a thin open ribbon-like channel of rectangular cross section with an aspect ratio (the ratio of width to height) over 80 so that channel walls can be closely approximated as two infinite, parallel plates [23, 24]. Flow between parallel plates separated by small distances is laminar for the flow velocities of interest and is described by

$$v = \frac{wy - y^2}{2\eta}\frac{\mathrm{d}p}{\mathrm{d}x} = 6\langle \mathrm{v} \rangle \left(\frac{y}{w} - \left(\frac{y}{w} \right)^2 \right), \tag{1}$$

where, v is the flow velocity at a distance y from one of the plates, η is the viscosity of the fluid, w is the plate separation or channel height, $\langle v \rangle$ is the average flow velocity across the channel, and $\mathrm{d}p/\mathrm{d}x$ is the pressure gradient along the flow axis. As the parabolic distribution given in equation (1) implies, the fluid velocity at the surface of the channel walls is zero (nonslip flow) while at a maximum in the center of the channel. Thus, if a particle or cloud of particles were to maintain an average distance y different from another particle or cloud of particles, their average velocities through

the channel would be different and they would exit the channel at distinct times.

Retention in FFF is the measure of the ability of the system to retain or retard the travel of a particle through the channel compared to a particle unaffected by the applied field. Experimentally, the retention ratio R is found by

$$R = \frac{t_0}{t_r} = \frac{V_0}{V_e}, \tag{2}$$

where t_0 is the time required for an unretained particle to exit the channel, t_r is the time for the retained sample to exit, V_0 is the void volume of the channel, and V_e is the elution volume of the sample. The elution or retention time in FFF is directly related to the properties of the sample and the sample's response to the applied field according to the equation [20]

$$R = 6\lambda\left[\coth\left(\frac{1}{2\lambda}\right) - 2\lambda\right], \tag{3}$$

where λ is a nondimensional parameter given by

$$\lambda = \frac{l}{w}. \tag{4}$$

The l in (4) is the average distance of a sample particle from the accumulation wall as described earlier and is related to experimental conditions by

$$l = \frac{D}{U}, \tag{5}$$

where D is the particle diffusion coefficient and U is the field-induced drift velocity, which depends on the applied field strength according to

$$U = \frac{S'\phi}{f'}, \tag{6}$$

where S' is the applied field strength, ϕ is the field susceptibility of the particles, and f' is the sample friction coefficient. Note that the form of (6) will vary somewhat depending on the type of field used in the particular FFF system. The diffusivity, D, can be calculated using the Einstein equation

$$D = \frac{\kappa T}{3\pi\eta d}, \tag{7}$$

where κ is Boltzmann's constant, T is the absolute temperature, and d is the particle diameter.

The balance between field-induced migration and diffusion away from the accumulation wall leads to an exponentially defined particle distribution

$$c(y) = c_0 e^{-\left(y\frac{U}{D}\right)}, \tag{8}$$

where $c(y)$ is the concentration of particles at a distance y from the accumulation wall and c_0 is the concentration of particles at the wall. Note that this particle distribution is only true for normal mode FFF and can be modified significantly if the retention is occurring in another mode of FFF.

Other effects that may cause deviations from this theory are typically referred to as repulsion effects. Studies on repulsion effects by Tri et al. have been reported for macroscale FFF systems [25]. Miniaturization of FFF channels may be limited by such particle–wall repulsion effects as these interactions typically result in the exclusion or the repulsion of the particles away from the accumulation wall and, hence, reduce the effective retention in FFF channels. These particle–wall interactions include electrostatic forces, hydrodynamic lift, and van der Waal's attractive forces. The wall repulsion layer increases the average particle cloud thickness l and can lead to incorrect measurements of sample properties. To fully understand scaling in FFF and the potential of FFF channel miniaturization, a thorough investigation in wall–particle and particle–particle interactions is needed.

2.3. Plate Height

In considering the usefulness and effectiveness of microscale FFF systems, figures of merit for comparing different FFF instrument designs and for comparing FFF instruments to other instruments are required. These figures of merit are generally based on the chromatographic concept of plate height. Thus a brief review of chromatographic plate theory follows.

The length L of a separation column can be broken down in to N theoretical plates of height H

$$H = \frac{L}{N}, \tag{9}$$

where the plate height, H, is a measure of variance (σ^2) or spreading that has been created as the band of particles being separated moves through the separation channel. The plate number, N, is a measure of the separation

efficiency of a system and indicates the number of times a certain separation level is accomplished in a channel. H can be closely approximated by the ratio of variance to the length of the channel, L, [26] according to

$$H = \frac{\sigma^2}{L}. \tag{10}$$

The plate height generally represents the length of the separation column required to generate a defined level of separation between two particles. Ideally, H should be as small as possible to maximize the level of separation between two samples generated in a given instrument. In chromatography systems, H and N are used as figures of merit for comparison with various instruments, with the goal being to minimize H and maximize N. Systems with a large plate height will have widely dispersed sample bands and will be unable to separate as many different samples simultaneously as an instrument with a small plate height. The goal in microscale systems is to minimize the plate height.

Plate heights in FFF are generated by a combination of factors such as nonequilibrium effects (H_n), longitudinal diffusion (H_d), sample relaxation (H_r), sample polydispersity (H_p), sample volume (H_s), and instrumental effects (H_i) [26]. These factors can be classified in two groups based on their origin. The first group contains effects that give rise to diffusion-based dispersion such as nonequilibrium effects and longitudinal or axial diffusion. The second category encompasses all other band-broadening factors that include sample and instrumental related effects. Sample relaxation, injection volume, polydispersity, and instrument-related plate height are included in this second category. Overall plate height, H, can be formulated as a combination of all of these factors [26] and written as

$$H = H_d + H_n + H_r + H_p + H_i + H_s. \tag{11}$$

Polydispersity of a sample is an inherent property of the sample being processed, not a system property, and can be ignored when optimizing an instrument. As diffusion coefficients are relatively low compared to the length of a FFF channel, the contribution of diffusion to plate height is negligible unless very low flow velocities are used. Thus, only the contributions due to geometrically dependent nonequilibrium and instrumental effects require consideration during microscale instrument design and optimization efforts.

2.3.1. Nonequilibrium Plate Height

In FFF, the nonequilibrium component of plate height, H_n, is heavily dependent on channel thickness, diffusion, D, and average flow velocity, $\langle v \rangle$ and is given by

$$H_n = \frac{\chi(\lambda) w^2 \langle v \rangle}{D}. \tag{12}$$

The function $\chi(\lambda)$ is highly complex and an exact derivation was found by Giddings [27] and so an approximation proposed by Giddings is mentioned here

$$\chi(\lambda) = 24\lambda^3 \left(1 - 8\lambda + 12\lambda^2\right). \tag{13}$$

H_n is a complex function of the channel dimensions and the effect of miniaturization on it can not be inferred directly. A closer look at the scaling of H_n is required to estimate the effects of miniaturization on plate height.

2.3.2. Instrumental Plate Height

In FFF systems, the instrumental component of plate height depends on the instrument setup, channel geometry, the fluidic connections, postcolumn volumes, and the sample injection size and method. These elements that contribute to instrumental band broadening are not easily expressed in a comprehensive theory and so have been ignored when examining these systems mathematically and conceptually. Thus, no comprehensive theory of instrumental effects exists and the effect of geometry on instrumental plate height is only known conceptually.

2.4. Resolution

The resolution of a chromatography system, R_s, is a measure of the relative separation ability of a system and can be represented by [21]

$$R_s = \frac{\Delta R}{4\bar{R}} \sqrt{\frac{L}{H}} \tag{14}$$

where ΔR is the difference in retention ratio for two distinct particles and $\bar{R}$ is the average retention ratio of the two particles being considered.

3. Miniaturization Effects in FFF

FFF can be classified in two broad classes based on the type of field involved. Typically, general FFF systems (e.g. sedimentation, flow, gravitational) fall in to the "nongradient based FFF" category where the field does not depend on the channel height, as is evident in the definition of the retention parameter λ. The miniaturization of such systems was not favored in the early FFF literature as resolution is expected to drop with miniaturization [28, 29]. It was generally believed that field strength manipulation could be used to increase the separation efficiency of the system by modifying the average particle cloud thickness in the channel, so miniaturization was unnecessary. A closer examination of the geometric scaling effects in recent times has shown that miniaturization of nongradient-based FFF systems can lead to a minimal loss in performance with possible improvement in certain situations for these FFF systems [29]. But in certain FFF subtypes (e.g. electrical and thermal), field strengths can not be increased indefinitely. Interestingly, the field experienced by particles in these systems is highly dependent on the channel thickness w. These FFF systems are classified as "gradient-based FFF" where the field scales with the channel height and an increase in field strength is expected with miniaturization. Electrical FFF (ElFFF) and thermal FFF have both shown improvement in retention with scaling. Miniaturization of FFF instruments has resulted in a reduction of the instrument size, sample and carrier volumes, and power consumption along with a reduction in analysis time, but the effect of miniaturization on FFF performance can only be determined by examining scaling behavior of plate height and resolution. Both nongradient and gradient-based FFF systems behave differently when miniaturized due to the contrasting dependence of plate height and resolution on channel dimensions.

3.1. Instrumental Plate Height

The packaging or interfacing of microscale FFF systems with the real world requires far more consideration than is needed for macroscale FFF channels. Typically, macroscale FFF systems use large flow cells for detectors, long lengths of extracolumn tubing, and large sample injection volumes. While the performance of macroscale systems does not get deteriorate considerably in these situations, it can severely affect microsystems. The effect of these large extracolumn volumes and sample sizes is referred to as instrumental effects. Such instrumental effects can play a large role in increased plate heights and a subsequent loss in resolution for microscale FFF systems. As the FFF channels are miniaturized, the importance of instrumental plate

height increases further. Typically, ultralow volume sample injections and on-chip detectors are preferred in conjunction with microsystems to reduce plate heights and sustain miniaturization related advantages.

The effect of miniaturization on instrumental plate height can be measured using experimental plate height data collected from elution peaks obtained from similar experiments conducted in FFF channels of various sizes [29]. Instrumental plate height data collected from a variety of FFF instruments of different sizes indicates an empirical correlation between instrumental plate height and channel height as

$$H_{\mathrm{i}} = 3w\,. \tag{15}$$

It can clearly be seen that the instrumental plate height drops with a dncrease in channel height and the associated improvement in sample injection, channel fabrication, and detector arrangement [30]. With miniaturization, instrumental plate height drops linearly and can be a critical factor in the overall reduction in plate heights.

Accordingly, there appears to be a clear advantage to miniaturization of FFF systems with regard to instrumental plate heights.

3.2. Gradient-Based Systems

Gradient-based systems are the FFF subtypes in which the applied field scales with channel height. Electrical FFF and thermal FFF systems fall into this category. These types of FFF systems are believed to benefit from miniaturization the most.

3.2.1. Plate Height Scaling

The total plate height that can be measured or calculated theoretically is a sum of nonequilibrium and instrumental plate heights. Comparative scaling analysis of these three plate heights: total, nonequilibrium, and instrumental give us a gauge of relative importance. Figure 2a shows the estimates for ElFFF systems, which indicate that plate heights are dominated by nonequilibrium effects, which generate an exponential increase in plate height as w increases. It should be noted that in FFF systems nonequilibrium plate height is a strong function of the applied field also. For example, in the case of ElFFF with a 0.25% effective field strength, the value of H_{n} is very high, almost 10 times higher than H_i, but as field strength is increased to 1.25%, the relative magnitudes of the instrumental and non-equilibrium contributions become similar. Thus, even at relatively moderate field strengths in ElFFF, particularly for microscale ElFFF, a tight control over H_{i} is very

important, which can be achieved only with proper instrument design and operation.

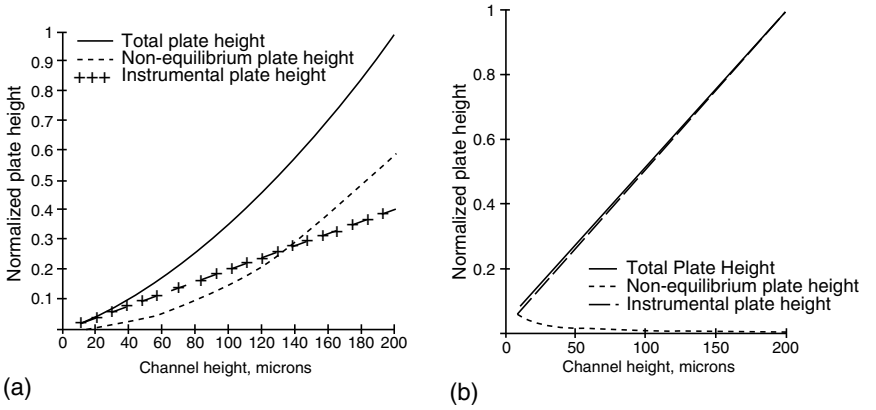

Fig. 2. Plots showing the variation of H_n and H_i with channel height for (**a**) Gradient-based systems (where field strength varies with w) and (**b**) general FFF systems (field is independent of w). Normalization was based on the highest value of the plate height in the dataset. Reprinted from Sant and Gale [29], Copyright (2006), with permission from Elsevier

3.2.2. Resolution Scaling

A general expression for resolution with a dependence on only a single geometric dimension can be obtained by making the length a function of channel height ($L = 3{,}000\ w$) and by substituting (3, 12, 13, and 15) into (14) (with total plate height as a combination of nonequilibrium and instrumental plate height) to obtain

$$R_s = \frac{\Delta R}{4\bar{R}}\sqrt{\frac{3000\bar{D}}{\chi\left(\bar{\lambda}\right)w\langle v\rangle + 3\bar{D}}}\,. \tag{16}$$

Note that (16) has the function $\chi(\lambda)$ embedded in it still (13) and that R and λ are also functions of w. The bar over variables in (16) indicates the mean values of the two particle clouds. These equations were used to provide a basic framework around which the various scaling effects associated with FFF systems can be compared.

Figure 3 shows the typical dependence of resolution on channel height w, for an ElFFF system. It is clear that resolution increases with a decrease in w, which is the motivating factor for miniaturizing ElFFF systems [29].

For typical experimental conditions, the resolution is nine times higher with a 10-fold reduction in channel height.

It should be noted that a reduction in channel height is always accompanied by a reduction in length when small analysis times are envisioned (the lower curve in Fig. 3). When the channel length scales proportionally to width, we expect a drop in resolution, but a large reduction in overall analysis time is achieved. Also, there is close to a 20% error when resolution [29] is computed with $\chi(\lambda)$ values obtained from (13) instead of the exact equation derived by Giddings [27].

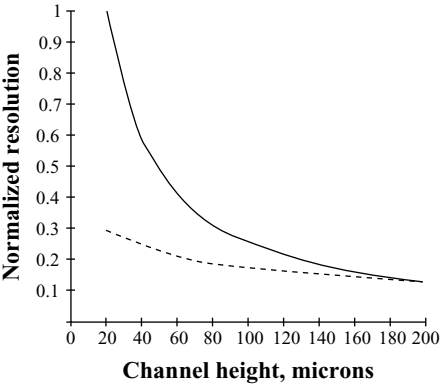

Fig. 3. Geometric scaling models for ElFFF system using a constant length of 60 cm. The assumed diameter and electrophoretic mobility of particles for the simulations are 50 nm and -1.75×10^{-11} m^2 $V^{-1}s^{-1}$. (*solid line*) Equation (16) with constant L and zero H_i, (*Dotted line*) Equation (16) with scaling L and scaling H_i. Reprinted from [29], Copyright (2006), with permission from Elsevier

3.3. Nongradient-Based Systems

3.3.1. Plate Height Scaling

Fig. 2b shows how plate height changes as the channel size is reduced for general FFF/nongradient-based systems and demonstrates how the relative importance of nonequilibrium and instrumental effects has switched and why there is little motivation to miniaturize these systems if only nonequilibrium plate heights are considered.

In this case the nonequilibrium effect (which increases with a reduction in channel height) is almost negligible and the plate height is dominated by instrumental effects.

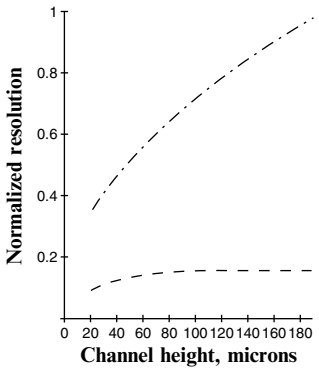

Fig. 4. Plot showing the effect of length and instrumental plate height on the resolution of general FFF systems as the channel height is reduced. (*Dashed line*) Equation (16) with constant L and zero H_i, (*Dashed-dotted line*) Equation (16) with scaling L and scaling H_i. Reprinted from [29], Copyright (2006), with permission from Elsevier

Unlike gradient-based FFF systems, mathematical models of general FFF systems predict a loss in resolution with miniaturization. The inclusion of instrumental plate height scaling, though, points to the possibility of an effective miniaturized general FFF channel. The top trace in Fig. 4 is the simulation result for normalized resolution (16) where L and H_i are kept constant at 60 cm and zero μm respectively, a typical geometry for general FFF systems. As expected, there is a considerable loss in resolution (~70%) when w is reduced to 20 μm, but there is also a 10-fold reduction in retention time – an advantage at a heavy price.

The bottom trace from Fig. 4 shows a nearly constant resolution if L and H_i scale with w, with only an 8% loss in resolution when w is reduced from 200 μm to 10 μm, while the 100 times reduction in retention time still occurs. This situation is the most likely one to be experienced in a practical situation, and provides evidence that miniaturization could be practical for general FFF systems [31].

Thus, a well designed general FFF should show improvement in resolution with miniaturization due to the major improvements related to instrumental effects. To gain all the advantages associated with miniaturization, though, general FFF systems may be required to operate under low retention conditions. The lower retention times associated with the high retention ratio will result in the reduced overall analysis time, while only sacrificing a small percentage of the potential resolution. Table 1 summarizes the scaling behavior of important FFF parameters and whether it is an advantage or disadvantage for both gradient and nongradient-based (general) FFF systems [32].

4. Microscale Electrical FFF

Electrical FFF was the first FFF subtype to be miniaturized using MEMS techniques [33]. In ElFFF, a voltage is applied across the two channel walls bounding the FFF channel [25, 34]. The separation criteria is based on the ζ-potential or electrophoretic mobility possessed by the particles suspended in the carrier solution, which is typically DI water or a low ionic strength buffer, a potential challenge when analyzing certain biological materials. With the ability to measure the electrophoretic mobility of sample particles with known sizes, ElFFF can be used both as a separation unit or a diagnostic instrument.

Applications of ElFFF include the following: separation of cells and organelles, bacteria and viral separations, characterization of emulsions, liposomes, and other particulate biological vehicles, separation of macromolecules, environmental monitoring, and biomaterial studies. ElFFF has been used to study protein adsorption by analyzing surface-modified particles for biomaterial applications. In addition to many of these appli-

Table 1. Nongradient FFF and gradient-based FFF parameters affected by miniaturization [32]

Parameter	General FFF scale factor	Advantage or disadvantage	ElFFF scale factor	Advantage or disadvantage
Retention ratio (R)	1/s	Disadvantage	1	Potential Advantage
Analysis time	s^2	Limited Advantage	s	Advantage
Drift velocity (U)	1	Neither	1/s	Advantage
Plate height (H)	1/s	Disadvantage	s^2	Advantage
Resolution (R_s)	s	Disadvantage	$1/\sqrt{s}$	Advantage
Steric transition (d_i)	1	Neither	$\sqrt{s}$	Potential Advantage
Equilibration time (τ_e)	s	Advantage	s^2	Advantage
Field time constant (τ)	N/A	Subtype Specific	s	Advantage
Required sample size	s^3	Advantage	s^3	Advantage
Solvent consumption	s^3	Advantage	s^3	Advantage
Instrument size	s	Advantage	s	Advantage
Separable particle size	s	Relative	s	Relative

cations, Gale et al. have employed μ-ElFFF in whole blood separations for medical diagnostics [35]. ElFFF also finds application as a sample pretreatment system by performing an initial separation on a sample that can later be collected for further testing by another analysis system. For example, ElFFF can be used as a sample preparation unit prior to a PCR step in a total analysis system.

A major advantage ElFFF enjoys over similar separation systems is low power and voltage requirements. In comparison to electrophoresis systems, which typically require several thousand volts, ElFFF operates below 3V. Even such a small amount of applied voltage across thin ElFFF channel results in a voltage gradient similar to that in electrophoresis systems that operate at about 1,000 times higher voltage. Thus, miniaturization proves beneficial in reducing power requirements and raises the possibility of a portable instrument with small batteries as power source.

4.1. Theory

Most of the general FFF equations can be applied directly to ElFFF by replacing U in the particular (5). For example, λ, the nondimensional parameter relating experimental parameters to R, is represented by

$$\lambda = \frac{D}{\mu E w} = \frac{\kappa T}{3\pi\eta\mu d E w}, \tag{17}$$

where μ is the electrophoretic mobility of the sample and product of E and w is effective voltage V_{eff}. Equation (17) shows that retention in ElFFF systems is still inversely proportional to w, but since the effective field E is also a function of channel height, there is no effect on retention as the channel is miniaturized. While this conclusion may seem to indicate that there is no net benefit in terms of retention from miniaturization, the fact that there is no disadvantage allows for the system as a whole to derive a significant advantage from miniaturization.

The steric transition point in FFF systems indicates a change in mode from normal FFF to steric FFF as defined earlier. The steric transition point in ElFFF systems can be determined using

$$d_{\text{i}} = \sqrt{\frac{2\kappa T w}{3 V_{\text{eff}}}}. \tag{18}$$

Examination of (18) suggests that the steric transition point for ElFFF systems is dependent upon channel height, a property significantly different from those of general FFF systems. Thus, by miniaturizing the system,

it becomes possible to significantly reduce the steric transition point and make available the high-speed separations possible in steric mode. The separation mode, though, cannot be changed to steric mode simply by increasing the applied field, as can be done in general systems, due to the electrolysis of water at even moderate applied voltages. Thus, for ElFFF systems, steric separations of smaller particles might be impossible unless channels with smaller dimensions are fabricated.

The mechanics of ElFFF are different from most other FFF systems due to the presence of the electrical field and its interaction with the aqueous carrier. An electrical double layer is created at the interface of the polarized electrode and carrier solution as shown in Fig. 5. A major portion of the applied field drops across this double layer resulting in an effective field in the bulk of the channel that is only a fraction of the applied voltage available for retention of the sample. Effective voltages on the order of 1% have been reported in case of μ-ElFFF systems [36, 37]. This loss of effective field is caused by two related electrochemical phenomena. First, a significant portion of the voltage drops at the electrode/carrier interface, which may be attributed primarily to the electrode material properties. Second, the applied voltage has to overcome a potential barrier before any significant charge-transfer starts between the electrode and the carrier solution. The severity of the effective field reduction depends largely on the thickness of the double layer or the ionic strength of the carrier solution. A compact double layer, as occurs with a high ionic strength carrier, may result in very low field in the bulk with little or no retention in the channel. A critical concern regarding miniaturization of ElFFF is the creation of a more compact double layer and relatively low ionic strength solutions that can be used in the systems.

If the effective field is very low, the first solution to solving the problem would be to raise the applied voltage. Unfortunately, since the electrodes are in direct contact with an aqueous carrier, at voltages over about 2 V, electrolysis occurs and bubbles are rapidly generated that destroy the flow profile and cause severe mixing that makes the system nonfunctional. Thus, applied voltages are generally proscribed to a value where electrolysis does not occur.

One of the major challenges in ElFFF is the determination of the effective field and its associated retention of sample in the ElFFF channel. Unfortunately, this problem is highly complex and involves a number of operational and instrument variables such as voltage, sample, carrier composition, pH and ionic strength, electrode material and history, and so on. Only a rudimentary model for simulating transport properties using the convection-diffusion equation has been presented by Chen et al. [38]. The convection-diffusion equation was used to mimic ion and particle transport (DNA with an anisotropic diffu-

sion coefficient) in ElFFF with an arbitrary value for the effective field (0.5% of applied voltage). The standard theory of ElFFF, though, embeds the solution to the convection-diffusion equation as illustrated by Palkar et al. [39] and numerical solution is not generally required if an effective field value is assumed, even for a sample with anisotropic diffusion. A more complete understanding of the inner workings of an ElFFF channel has not yet been presented.

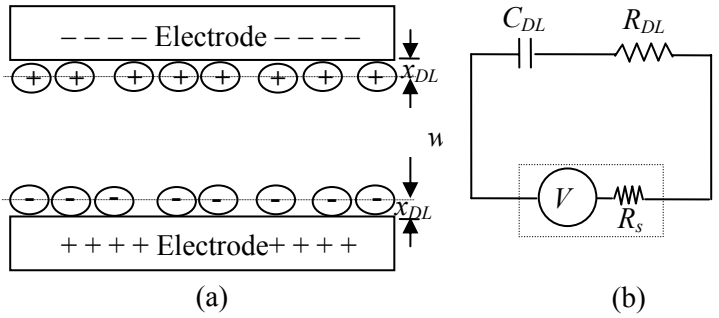

Fig. 5. (**a**) Electrical double layer in ElFFF system and (**b**) electrical circuit equivalent of ElFFF system showing double layer capacitance, source and bulk channel resistance, and voltage source

To get around this difficulty in understanding all of the processes taking place in the ElFFF channel, a way to predict ElFFF behavior based on an electrical circuit parameter model was developed by Kantak et al. [37, 40]. The ElFFF system can essentially be represented by electrical circuit components as shown in Fig. 5. In this model, the electrical double layer at each electrode can be represented by a parallel plate capacitor C_{DL} in parallel with the electrode–solution interface resistance R_{DL}. The effective potential responsible for separation in the channel is identified as the potential drop across the bulk resistance R_B. It should be noted that the bulk capacitance due to the channel itself will be very small at the low frequencies used in ElFFF (typically DC). R_s, the source resistance can play an important role in voltage distribution as will be described in more detail in the section on cyclical ElFFF. The value of each of these circuit elements can be measured experimentally with little difficulty and predictions of effective field and elution times made that are highly accurate.

Using the circuit in Fig. 5, an interesting observation regarding the speed of various configurations of ElFFF systems can be made. From basic electrical circuit analysis, the time constant for electric field stabilization, τ, of the system can be given as

$$\tau = \frac{(R_B + R_S)R_{DL}C_{DL}}{R_B + R_S + R_{DL}}. \tag{19}$$

Scaling analysis of the time constant reveals that a time constant of 40 s for a macroscale system drops to ~3.6 s for a similar microscale system, allowing a significant improvement in overall analysis time.

4.2. Fabrication and Packaging

Conventional semiconductor fabrication processes were applied towards fabrication of the earliest μ-ElFFF systems as outlined in Fig. 6 [33]. KOH etching was used to realize input and output ports on a silicon wafer. Titanium and gold layers were sputtered on the silicon as well as a glass substrate used as the second wall of the FFF channel. Platinum has also been used as an electrode material [37]. Thick photosensitive polyimide/SU-8 was photolithographically patterned to realize the microfluidic channels and provide a spacer between the electrodes. The two substrates were then bonded together to make an enclosed ElFFF channel. In several versions of the system, an adhesive trough was provided around the channel to facilitate adhesive bonding of the silicon wafer with polymer channel to a glass substrate with identical channel electrodes. For fluidic connections, PEEK tubing was attached to the silicon wafer over the ports using a ferrule glued to the substrate. Electrical connections were made by bonding wires to extensions of the electrodes. Another microfabricated system was reported by Lao et al., which used indium tin oxide (ITO) as electrodes [41]. ITO

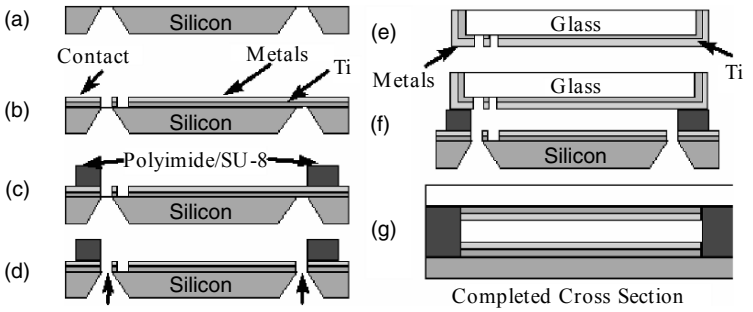

Fig. 6. Fabrication flow chart for the μ-ElFFF system. (**a**) Etching of input and output ports in silicon. (**b**) Deposition and patterning of titanium as adhesion layer and gold as channel electrode an. (**c**) Spinning and patterning of polyimide/SU-8 as channel walls. (**d**) Removal of Si_3N_4 membranes. (**e**) Deposition and patterning of titanium as adhesion layer and gold as channel electrode on glass. (**f**) Bonding of glass and silicon substrate using UV-curable adhesive. (**g**) Cross section of completed μ-ElFFF system

(transparent ceramic)-coated glass of 3 mm thickness was patterned to obtain electrodes with sheet resistance of 14 $\Omega\,cm^{-1}$. This manufacturing process also used SU-8 as channel walls.

For more recent microscale ElFFF systems, the fabrication process was modified so as not to include any special micromachining processes and yet still achieve the advantages related to the miniaturized systems. In this design, polished graphite plates were used as both channel electrodes and a microfluidic channel was cut in a 25-μm thick double side adhesive tape, using xurography, an inexpensive rapid prototyping tool based on knife plotting [42, 43]. This system provided more reproducible fabrication results in a cost effective manner and proved efficient in producing prototypes for research purposes.

Typical μ-ElFFF system geometrical dimensions are 6 cm length, 2 mm width, and 25 μm height in comparison to a macroscale channel of 64 cm length, 2 cm width, and 176 μm height. The sample injection for microsystem is reduced to 0.1 μL from a 1-5 μL for macroscale system.

4.3. System Characteristics

With the fabrication of the first microscale ElFFF systems an effort was made to understand the operation of these systems and compare the results to macroscale systems. These comparisons included basic electrical operation of the systems followed by retention and separation experiments.

The most basic characteristic for ElFFF systems is the current–voltage relationship. Typically, the currents are relatively small at low voltage values (<1.2 V for platinum electrode systems). Such low currents do not generate enough effective field to induce any retention of the sample. In the vicinity of 1.5 V, the current increase is approximately linear in proportion to voltage. This voltage is loosely termed the "turn-on" voltage and is a function of the overvoltage for electrode material [44]. This turn-on voltage changes with electrode system and the order of overvoltage for the systems we have tested are graphite < platinum < gold. At higher voltages, current growth slows indicating limiting charge transfer reactions.

Other important parameters for an ElFFF system include the electrical time constant and the required stop-flow/sample relaxation time. The measured time constants for the early microsystems measured from 1 to 4 s in comparison to 40 s for its macroscale counterpart. More recently, microscale systems have been shown to have time constants of less than 10 ms depending on testing method and the materials involved [45, 41]. The stopflow time in FFF is designed to allow the injected particles to move to their equilibrium positions, which reduces band broadening and

improves the retention characteristics. The equilibration time, t_e can be determined by [20]

$$t_e = \frac{w^2}{\mu V_{eff}}. \tag{20}$$

For macroscale systems, the stop flow time can be 5 min, but for microscale systems a stop flow time of only 2 to 3 s is sufficient.

4.3.1. Retention

Retention is directly related to current in ElFFF and a plot of the inverse of current with retention ratio λ, shows that retention in microscale systems follows the theoretical predictions and that a straight line through the data goes through the origin as shown in Fig. 7a [37]. Microscale ElFFF systems have been demonstrated for a range of samples, conditions, and configurations. An example of differential retention of particles based on a difference in electrophoretic mobility is shown in Fig. 7b.

A retention related ElFFF characteristic is size selectivity, which is a measure of a systems ability to separate based on size. Typically, macrosystems possess size selectivity between 0.67 and 1 [34], but size selectivity in microscale ElFFF has been shown to be close to unity [37].

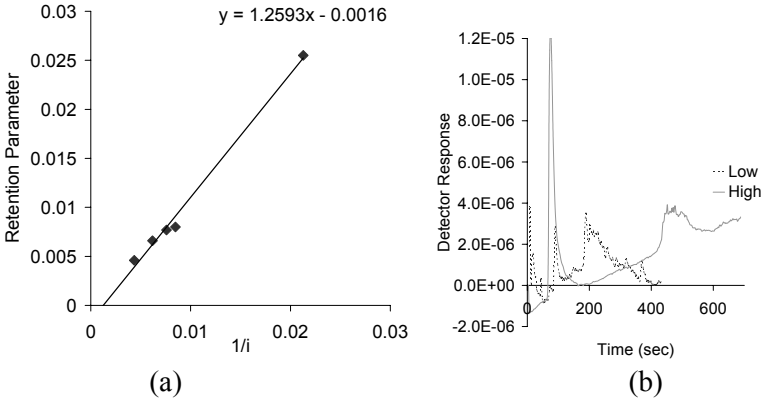

Fig. 7. Retention results in ElFFF [37]. (**a**) Graph of retention parameter, λ, compared to the inverse of the measured current, *1/i*. The experiments were performed using 94 nm PS particles in DI water with a flow rate of 0.3 mL/h in a system with platinum electrodes. (**b**) Fractograms of particles with the same diameter, but differing levels of carboxylation. The run labeled "low" had a lower density of COOH groups on the surface (67 μequiv g^{-1}) compared to the sample labeled "high" (510 μequiv g^{-1}). The carrier was DI water with a voltage of 1.392 V (10 μA) and a flow velocity of 1.48 mm s^{-1}. Reprinted with permission from Gale et al. [37]. Copyright (2002) American Chemical Society

The theory for FFF predicts that the steric transition point should fall as the channel is miniaturized, but this was found not to be the case. For a 28 μm channel μ-ElFFF system, the steric transition point was found to be 450 nm, which is similar to the limit for macroscale systems. While there may be potential for the steric transition point to be pushed to lower diameters, the likely reason for similar results is particle/wall repulsion effects [25], which would likely operate in a similar manner for both macroscale and microscale systems. While, the origins of the exclusionary effects are not well understood, they may be linked to particle–wall repulsion, frictional drag, and lift forces. It will be interesting to see how this exclusion zone scales and whether it becomes the limiting factor in the performance of microsystems.

4.3.2. Separations

A goal for μ-ElFFF is high-speed separations that can be detected using an on-chip detector [37], which should significantly reduce band broadening and maximize resolution. Figure 8a shows such a separation of a multicomponent polystyrene particle mixture in under 120 s. A separation of identical resolution in a macroscale system would require 2 h. As shown in Fig. 7b μ-ElFFF can also generate charge-based separation, an attractive feature for biological separations. Figure 8b demonstrates how identical particles with and without proteins attached to the surface can be differentially retained and separated in a μ-ElFFF system. Separations of blood components both before and after homogenization have been demonstrated using these same systems [35].

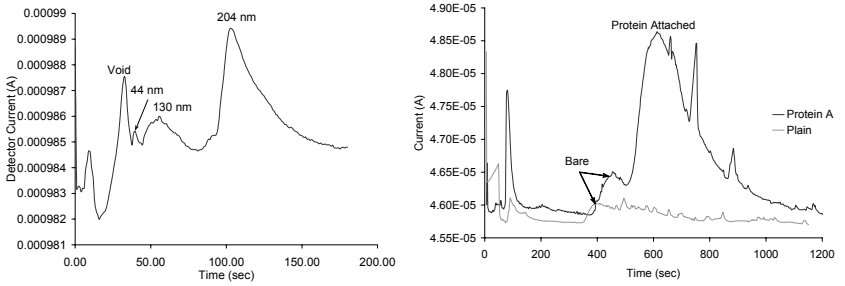

Fig. 8. Separations performed in microscale ElFFF system. (**a**) Separation of a mixture of polystyrene particles detected using an on-chip conductivity detector. The operating conditions are 1.6 V, 0.3 ml h^{-1} flowrate and 27 μA current in a 2-mm wide channel with platinum electrode with DI water carrier. Reprinted with permission from Gale et al. [37]. Copyright (2002) American Chemical Society. (**b**) Fractograms showing differential retention and separation between bare particles and particles with attached protein A [32].

The retention and separation data for μ-ElFFF was obtained with an on-chip conductivity detector [46, 47]. The on-chip conductivity detector was used to minimize the band broadening due to postcolumn volumes and to maximize the miniaturization related advantages of the μ-ElFFF channel. Another type of on-chip detection scheme employed with μ-ElFFF was based on the resonance light scattering (RLS) principle [48]. On-chip RLS is based on the shift in absorption and scattering spectral profiles for different particles, i.e., different sized particles yield different colored scattered light. The main advantages of this technique include the following: its noninvasive nature, high sensitivity for particle detection, and low cost.

4.3.3. Effective Field Scaling

The most important performance factor in ElFFF is the effective field. Since the effective field in the channel is difficult to determine using transport and electrochemical models, the effective field is usually calculated from retention data of standardized particles with known electrophoretic mobility. The effective electric field, E_{eff}, responsible for the given retention is then calculated using

$$E_{\text{eff}} = \frac{6Dt_{\text{r}}}{\mu w t_0} = \frac{2\kappa T t_{\text{r}}}{\mu w \pi \eta d t_0} . \tag{21}$$

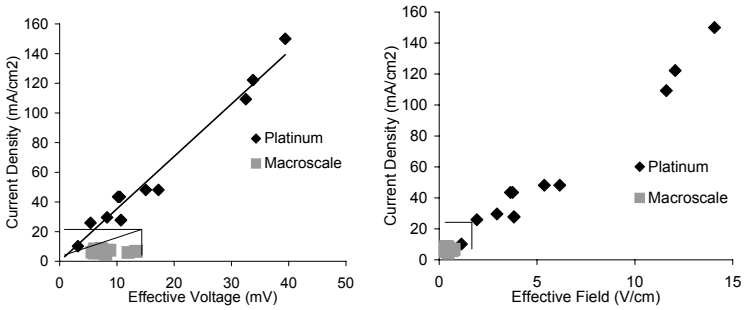

Fig. 9. Comparison of electrical properties of microscale and macroscale ElFFF system. The boxes in both figures represent the limits of the macroscale system. Plots show (**a**) effective voltage and (**b**) effective field as a function of current density for both systems. Platinum refers to data from a platinum-based microscale system. Reprinted with permission from Gale et al. [37]. Copyright (2002) American Chemical Society

The effective field calculated using (21) is generally only ~1% of the applied field. Figure 9 shows the measured effective field for a μ-ElFFF

system as a function of current density and shows that microscale systems significantly outperform macroscale systems, which are constrained to the boxes drawn in each figure. It can be seen that macroscale system is more efficient in terms of generating more effective field in comparison to microscale system for a given amount of current, but the amount of effective field that can be generated using a microsystem far exceeds that of a macroscale system. The limits in this comparison may be related to the electrode composition (platinum for microscale, graphite for macroscale) and similar data generated for graphite microsystems may show even better results.

5. Microscale Cyclical Electrical FFF

Once μ-ElFFF channels had been developed, efforts were made to determine methods to overcome the electrochemical limits associated with ElFFF. Cyclical fields were proposed as a way to overcome some of the capacitance associated with the double layer and drive effective fields up substantially. This method has proven very effective and has turned into a useful method worth considering on its own. Note that Cyclical Field-Flow Fractionation (CyFFF) was first proposed as a method by Giddings in 1986 [49] and demonstrated using a gravitational FFF system [50], but the only microscale systems have been cyclical electrical (CyElFFF). Thus, CyElFFF will be the focus of this text, though much of the analysis also applies to other CyFFF techniques.

Physically, a CyElFFF system is identical to an ElFFF system and both techniques can be performed using the same channel and electrode setup [51, 52]. As shown in Fig. 10, the mechanics of CyFFF are quite different from normal FFF due to the presence of the oscillating field.

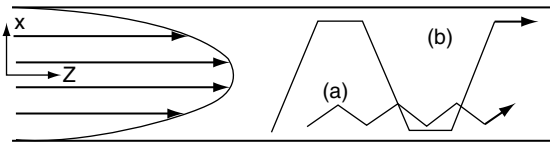

Fig. 10. Schematic diagram of the particle mechanics for (**a**) CyFFF mode I and (**b**) CyFFF mode III

Unlike normal ElFFF, the particles interacting with the field do not reside near the accumulation wall or form a static exponential concentration

profile (Fig. 10a) but move back and forth between the parallel electrodes under the influence of cyclical field. A number of operational and physical parameters (applied voltage and its frequency, electrophoretic mobility and size of the particles, flow rate, pH, and ionic strength of the carrier solution) determine how fast and how far the sample particles move between the electrodes and the average location of the particles in the channel. Depending on the motion of the particles, a particular group of particles will spend more or less time in the faster velocity zone (away from the channel electrodes) compared to other particles, generating differential retention and separation.

Based on the magnitude of the particle movement between the channel electrodes, CyElFFF can be classified into three different modes of operation. If particles oscillate only against one wall/electrode and do not completely cross the channel and reach the other wall, the particles are operating in Mode I. If the particles completely cross in one half cycle and rest for some period against the opposite wall, the particles are operating in mode III. Mode II occurs when particles reach the opposite wall just as the field is reversed.

5.1. Theory

In CyElFFF the retention ratio, R can be related to a nondimensional parameter λ_0, which for an applied square wave electrical field is given by

$$\lambda_0 = \frac{\mu E_{\text{eff}}}{2fw} = C\frac{\mu E_{\text{eff}}}{fw^2}, \tag{22}$$

where f is the frequency of the field oscillation in Hertz. λ_0 values can be used to determine the mode of CyElFFF operation and retention ratio R. For mode I, R is given by

$$R = 3\lambda_0\left(1 - \frac{2\lambda_0}{3}\right) \text{ for } \lambda_0 \le 1; \tag{23}$$

whereas, for Mode III R is given by

$$R = \frac{1}{\lambda_0} \text{ for } \lambda_0 \le 1. \tag{24}$$

Mode II can be represented by either model as the unity value of λ_0 holds true for both (23) and (24).

Equations (22) to (24) were first developed by Giddings [49]. Gidding's model does not account for three factors related to FFF, which can

occasionally be significant: steric effects due to finite particle size, diffusion effects, and, in CyElFFF, the reduced effective field due to the electrical double layer induced shielding. In reality, when a spherical particle approaches an accumulation wall, it cannot get any closer than its radius where the center of mass is located. Because of this steric effect, particles never have a truly zero velocity, and hence, retention times are less than predicted. Particle diffusion across the channel (*x*-direction in Fig. 10) can change the resultant average particle location in the channel and hence, the elution time. Finally, the presence of the electrical double layer should reduce the effective field for CyElFFF, creating a host of challenging problems.

These three major modifications to the CyElFFF theory were made by Kantak et al. [40] with a few assumptions and using a single model particle in the improved CyElFFF model. The assumptions made were (a) no overlap of electrical double layers for particles and electrodes, (b) no frequency dependence of particle double layer, (c) constant particle electrophoretic mobility, (d) except for the diffusion modeling, coherent particle motion that can be represented by a single particle, and (e) a relaxed sample with motion starting at one of the accumulation walls. This model was found to closely predict the elution times of particles, as will be shown later.

5.1.1. Effective Field Model

There are several ways that the effective field distribution in ElFFF or CyElFFF channel can be computed. Biernacki et al. [53] and Chen et al. [54] used a first principles approach to compute effective field from transport models of ions and particles. A combination of Poisson's and the Nernst-Planck [53] or the convection-diffusion equations [54] were used to model the particle and ion movement in the channel. While, this approach should result in a very generic model that can be applied to any situation concerning CyElFFF operation, the field values used in both these models were arbitrary and did not take into account the electrochemical processes occurring at electrodes and electrode-carrier interface. A complete model of CyElFFF should actually account for all electrochemical kinetics and species transport without any empirical quantities.

Another approach to compute effective field is by using the electrical analog of CyElFFF (Fig. 5) [40]. Using basic electronics principles the effective field across the bulk of the channel can be predicted by

$$E_{\text{eff}} = \frac{VR_{\text{B}}}{w}\sqrt{\frac{1+(2\pi f R_{\text{DL}}C_{\text{DL}})^2}{(R_{\text{B}}+R_{\text{S}}+R_{\text{DL}})^2+(2\pi f(R_{\text{B}}+R_{\text{S}})R_{\text{DL}}C_{\text{DL}})^2}}\,. \tag{25}$$

The circuit parameters required to calculate effective field can be measured using a simple series of experiments [40]. Thus a semiempirical model of CyElFFF can be generated by using the experimentally derived electrical circuit parameters towards predicting effective field in the system using (25).

5.1.2. Steric Effects in CyFFF

The main contribution of steric effects is in limiting the approach of particles to the accumulation wall. To account for the steric effects in CyFFF, one has to include the size of the particle while calculating the particle displacement in the channel. Making the adjustment for steric effects, the retention in CyFFF systems for Mode I and III are then given by

$$R_{\mathrm{I}} = 3\lambda_o\left(1-\frac{2\lambda_0}{3}\right)-6\frac{d}{2w}\left(1-\lambda_0-\frac{d}{2w}\right) \text{ and} \tag{26}$$

$$R_{\mathrm{III}} = \frac{(w-d)}{\lambda_0 w}\left(1+\frac{d}{w}\left(1-\frac{d}{2w}\right)\right)+6\gamma\frac{d}{w}\left(\frac{1}{2}-\frac{(w-d)}{2w\lambda_0}\right) \tag{27}$$

respectively, where γ is a dimensionless correction factor accounting for particle migration under steric conditions [55] and is between 0.5 and 1.0.

5.1.3. Particle Diffusion Effects

For mode I where particles just oscillate near one of the channel walls, diffusion in the x-direction can be critical as it significantly affects the location of the particle clouds and in turn elution times. For coherent motion of particles, linear unidirectional diffusion length of a single particle can be obtained from random walk theory as

$$l_{\mathrm{D}} = \sqrt{2Dt}\ . \tag{28}$$

The diffusion displacement in the x-direction, x_{D}, with a geometric factor for the centroid of the particle cloud is given by

$$x_{\mathrm{D}} = \frac{4\sqrt{2Dt}}{3\pi}\ . \tag{29}$$

For mode III CyElFFF begins to approach normal FFF at high values of λ_0, and diffusion can begin to play a role. If steric effects are not controlling, the distance traveled by the particle (z_{III}) along the channel (z-direction) is given by

$$z_{\mathrm{III}} = 6<v>\left(\frac{(w-2l)}{2\mu V_{\mathrm{B}}}+\frac{(w-2l)l}{\mu V_{\mathrm{B}}}-\frac{(w-2l)}{3w\mu V_{\mathrm{B}}}-\frac{(w-2l)l}{w\mu V_{\mathrm{B}}}-\frac{(w-2l)\ l}{w\mu V_{\mathrm{B}}}\right) \tag{30}$$

$$+\,6<v>\left[\frac{1}{2w}-\left(\frac{1}{2w}\right)^2\right]\left(\frac{1}{2f}-\frac{(w-2l)w}{\mu V_{\mathrm{B}}}\right).$$

It should be noted this lumped electrical parameter model does not account for all potential physical effects and for this reason, the scope of this model can be limited and should be used with care [40, 45].

5.2. Experimental Results

CyElFFF has shown the ability to significantly retain nanoparticles and to perform separations on nanoparticles, especially using low ionic strength carriers. Examples of some of these experiments are summarized in the following sections.

5.2.1. Comparison of Theory with Experimental Data

Figure 11 shows the typical elution characteristics of the μ-CyElFFF as a function of frequency of the applied field [40]. It can be deduced from Fig. 11 that Giddings's model clearly does not match with the experimental data and deviates even with the inclusion of steric and diffusion effects. Elution times computed using the estimated effective field instead of the nominal field yield a better match with the experimental results and show that electrical double layer related effects are of prime importance in CyElFFF. Also, mode transition can be predicted correctly with the use of the lumped electrical parameter model for the evaluation of λ_0.

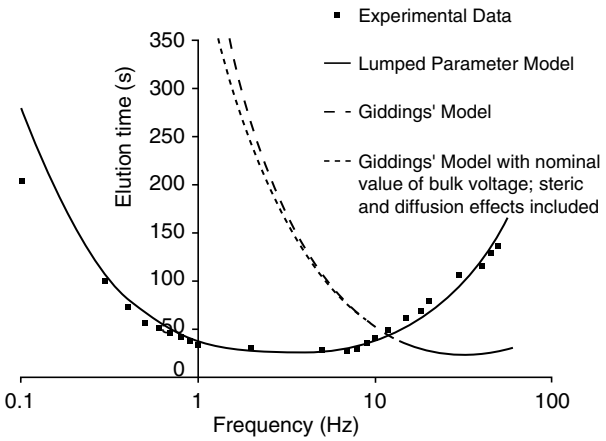

Fig. 11. Comparison between model and experimental model for μ-CyElFFF system. Reprinted with permission from Kantak et al. [40]. Copyright (2006) Wiley nanoparticles in a 50 μM ammonium carbonate carrier

Lao et al. showed that the increased effective field with the pulsed field resulted in 50-fold increase in current and that there was a strong influence of pulse frequency on retention time [41]. The retention dependence on voltage is straightforward and an increase in applied voltage results in increased retention when in Mode III. For example, the elution time quadruples when the peak to peak voltage (square wave at 1 Hz) is increased from 1 to 8 V for retention of 100 nm amino-coated polystyrene nanoparticles in a 50 μM ammonium carbonate carrier.

5.2.2. Separations

Separations in μ-CyElFFF are dependent on a difference in the electrophoretic mobility of the samples. In the earliest separation results published by Lao et al., pulsed ElFFF, a variation of CyElFFF, was able to resolve 0.105 μm and 0.405 μm particles [41].

Figure 12 shows high-speed separations (<3 min) of nanoparticles using μ-CyElFFF [52]. It can be seen that resolution is highly dependent on frequency and in this case separation resolution increases with the frequency of the applied field. It should be noted that plate heights also vary with frequency and tend to follow a pattern similar to the elution times (Fig. 11) with a minimum plate height obtained near the mode transition point. This translates to limits on separation power in μ-CyElFFF with reduced peak capacities in comparison to μ-ElFFF. An offset voltage is used to force the particles towards one accumulation wall while operating in mode I to relax the sample and avoid initial random distribution of the particles across the channel height.

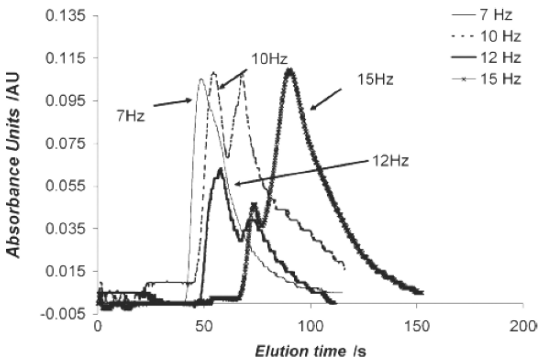

Fig. 12. Separations of 100 nm silica nanoparticles (first peak) and polystyrene (PS) amine group nanoparticles (second peak). The operating conditions are a square wave of 3.0 VPP with 0.3 VDC offset, DI water as carrier with 1.0 mL h^{-1} flow rate [52]. Reproduced by permission of The Royal Society of Chemistry

5.2.3. Effects of Carrier pH and Ionic Strength

The ionic strength of the carrier affects the retention characteristics and effective field of the CyElFFF to a great extent. Bulk channel conductivity, double layer impedance, current across the channel, electrophoretic mobility of the particles, and source resistance all are affected at various levels across the frequency spectrum of the applied field [45].

In general an increase in current associated with an increased ionic strength correlates to a drop in available effective field, while an increase in current for constant carrier conditions results in an increase in effective field. Similar logic applies to an increase in pH. It should be emphasized that in order to obtain reliable operation using either ElFFF or CyElFFF, the carrier conditions should be maintained carefully. Also, the electrophoretic mobility increases with an increase in ionic strength [56]. The overall effect of increased electrophoretic mobility and reduced effective field results in very convoluted CyElFFF retention results with increase in ionic strength as shown in Fig. 13. Not only does retention drop, but the band broadening of the elution peaks also increases with an increase in the ionic strength of the carrier, leading to very poor results.

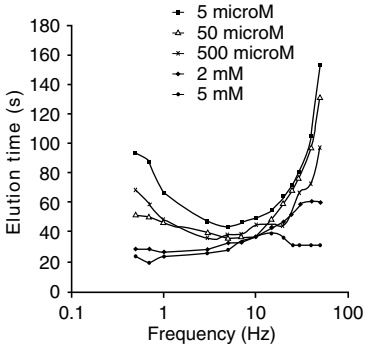

Fig. 13. Retention characteristics of μ-CyElFFF as a function of ionic strength of carrier and frequency of the applied oscillating field. Reprinted with permission from Kantak et al. [45]. Copyright (2006) American Chemical Society

Microscale CyElFFF has shown promise as a nanoparticle separation and analysis technique with the ability to generate significant retention and high electric fields in both Mode I and Mode III. The primary limitation of the technique is that it does not work well with high ionic strength carriers.

6. Microscale Dielectrophoretic FFF

Pioneering work on microscale dielectrophoretic FFF (DiFFF) was done by Gascoyne's group with applications in cancer research and cell separations [57–63]. These systems are technically Dielectrophoresis-Gravitational FFF systems in which dielectrophoretic (DEP) fields are used to drive particles away from the wall and gravitational forces drive the same particles towards the wall, similar to hyperlayer FFF. Thus a balance between these competing fields determines the average particle location in the channel and the elution time.

DiFFF devices were created using a combination of microfabrication and conventional FFF assembly techniques. Fabrication of the electrodes to impart the dielectrophoretic field requires the use of microfabrication techniques. Standard photolithography techniques were used to manufacture interdigitated electrodes of 50 μm in both width and gap on a glass substrate [59]. A Teflon spacer of 400 μm thickness was cut to realize an open channel of 50 mm width with 288-mm tip to tip length. A set of 36 nylon screw-clamps were used to assemble the DiFFF chamber with the Teflon spacer being sandwiched between two glass substrates. The glass substrate allowed optical interrogation of the sample as it passes through the FFF channel. For cellular separations, use of a fraction collector is a common practice enabling the user to perform more diagnostic tests on the individual fractions.

6.1. Theory

Figure 14 shows the operational principle of DiFFF and the forces involved in this separation technique. Dielectrophoretic forces are generated

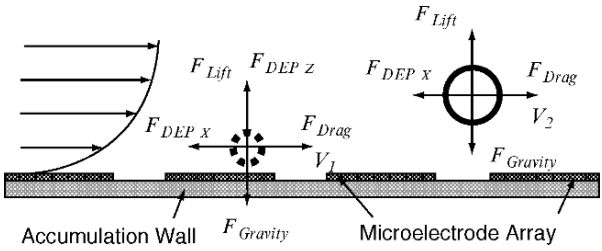

Fig. 14. The DiFFF principle. A close look at the accumulation wall shows the parabolic velocity profile, the microelectrode array and two particles with different dielectric properties at different locations away from the accumulation wall determined by a force balance of DEP levitation, hydrodynamic lift, gravity, and fluid flow-induced drag

by a nonuniform AC field imparted by electrodes on one wall of the channel [60]. For dielectrophoretic separations, polarizability of the particle plays an important role as the sample particles are suspended in an aqueous medium in the presence of a high frequency electric field. Electrostatic interactions between polarized particles and the field induce movement of the particles. The degree of polarizability and the particle's size cause a particle to experience different relative forces away or towards the channel walls, which induces a unique velocity along the channel, as is typical for FFF. In addition to the particle properties, the carrier properties (aqueous medium), and the frequency and magnitude of the applied field help determine the forces on a particle. If the particle polarizability is less than that of the medium, particles experience negative DEP forces and are moved away from the high field strength area. In positive DEP particles are retained near the electrodes where high field strength zones are located. Both of these types of DEP are very useful and can be employed to separate particles if proper elution modes are used. Depending on the particle properties, two different types of DEP modes: migration and retention can be used. In DEP migration mode, different types of sample particles with polarizability on either side of medium are separated. Positive DEP causes retention of one type of particle at the electrodes and the particles experiencing negative DEP are forced away from the electrode region (into faster flow lines typically) to achieve spatial separation across the channel. DEP retention mode utilizes the balance between DEP and hydrodynamic forces to realize discreet retention of the sample particles. Particles that experience positive DEP are retained strongly at the electrode surface and particles with weak interaction forces (small positive DEP or even some negative DEP) elute earlier. This mode of DEP maintains the particles at different heights and is the most common mode used in DiFFF [59]. Retention mode DiFFF has the potential to obtain higher resolution than migration mode DiFFF due to inherently higher selectivity as it requires smaller differences between the dielectric properties of cells to generate a significant retention difference.

The electrodes used to impart the dielectrophoretic force field are typically interdigitated to generate nonhomogeneous field. Particles with different polarizabilities levitate in distinct velocity zones under the influence of the collective electrical and hydrodynamic/gravitational forces. Typically, the resultant $F_{\text{DEP-X}}$, dielectric force component opposing the carrier flow is very small compared to the $F_{\text{DEP-Z}}$ acting in the perpendicular direction, especially since the horizontal force averages out due to the interdigitated nature of the electrodes. For the particle sizes typically involved in DiFFF, gravitational and lift forces are also significant. Forces describing the physics behind dielectrophoresis can be summarized by equations (31) to (35), where V_{RMS} is

$$F_{\mathrm{DEP_Z}} = 2\pi\varepsilon_{\mathrm{m}} r^3 p\,\mathrm{Re}\left(f_{\mathrm{CM}}\right) q(h) V_{\mathrm{RMS}}^2, \tag{31}$$

$$F_{\mathrm{gravity}} = \frac{4}{3}\pi r^3 \left(\rho_{\mathrm{p}} - \rho_{\mathrm{m}}\right) g, \tag{32}$$

$$F_{\mathrm{Lift}} = C\frac{6\eta r^3 \langle v \rangle}{w(h-r)}, \tag{33}$$

$$\mathrm{Re}\left(f_{\mathrm{CM}}\right) = \frac{f^2 - {f_0}^2}{f^2 + 2{f_0}^2}, \tag{34}$$

$$f_0 = \frac{\sigma_{\mathrm{m}}}{\pi r C_{\mathrm{mem}}}, \tag{35}$$

the applied RMS voltage, ε_{p} and ε_{m} are the particle and medium dielectric permittivities, ρ_{p} and ρ_{m} are the particle and medium densities respectively. $\mathrm{Re}_{(\mathrm{fCM})}$ is the real part of the Clausius-Mossotti factor f_{CM}, which is a function of the frequency-dependent complex dielectric permittivities of the particle and the medium and essentially reflects the frequency dependent magnitude and direction of the field-induced polarization $\alpha_{\mathrm{DEP(f)}}$. f_0 is the crossover frequency at which DEP forces acting on the cells are zero, C_{mem} is the membrane capacitance, and σ_{m} is the electrical conductivity of the cell-suspending medium. The capacitance difference due to membrane surface area has more effect on cell separation mechanics than the membrane composition or morphological differences. *q(h)* is the measure of height dependence of F_{DEPZ}, *p(f)* is a frequency-dependent factor to account for the electric double layer induced voltage drop, *h* is the position of the particle, *r* is the particle radius, $\langle v \rangle$ is the average velocity of the fluid, and *C* is a constant (0.172). An expression for the levitation height of the sample can be derived by combining and simplifying (31)–(33) as

$$h_{\mathrm{eq}} = \frac{1}{q(h)}\left(\frac{2\left(\rho_{\mathrm{p}} - \rho_{\mathrm{m}}\right) g - {3F_{\mathrm{Lift}}}/{2\pi r^3}}{3\varepsilon_{\mathrm{m}} p(f)\,\mathrm{Re}(f_{\mathrm{CM}}) V_{\mathrm{RMS}}^2}\right). \tag{36}$$

Typically, the geometrical dimensions of the dielectrophoretic chamber are limited by the size of sample being processed. As DiFFF was developed to analyze cells, channel thickness is generally 250–400 μm. Since retention in DiFFF is partially a function of the channel height, work on optimization of channel dimensions would be of interest for future miniaturization efforts.

6.2. Experimental Results

DiFFF was used to separate human leukemia (HL-60) cells from normal human mononuclear cells, polystyrene beads with different surface properties, and human breast cancer cells from whole blood. Excellent separation results were obtained for a variety of cell types that closely match with the theoretical models proposed for them [57, 58, 63].

For a typical experiment, the DiFFF channel was loaded with sucrose buffer and leukocyte samples were loaded using an injection valve [63]. A 10 kHz DEP voltage (4 V peak to peak) was applied to the electrodes during loading of the cells to prevent adhesion of the cells to the electrode surface. Cells were allowed to sediment towards the DEP electrodes in the chamber for 5 min. Table 2 is the summary of leukocyte analysis results using DiFFF.

Field programming in terms of the use of a combination of swept frequency and fixed frequency improves the discrimination of the different cell types. Details of these experiments are available [57, 58, 63].

Similar separations of human breast cancer cells (MDA-435) from normal T-lymphocytes resulted in 99.2% purity after separation within 11 min with a close to 69% total cell recovery [58].

It can be seen from Fig. 15 that most of the breast cancer cells were retained near the electrode channel under positive DEP at 20 kHz as only 35% of cells elute from the channel. These results suggest that designing the experimental conditions (mainly frequency) for different types of cells is an important issue. The effect of voltage on each cell type was similar, so voltage cannot be used to aid the selectivity of the system.

Table 2. Summary of leukocyte separation by DiFFF

Experimental parameters	Cell types	% Purity	Separation time (min)
Monocyte: T-lymphocytes (20–50 kHz, 10 min: 5 kHz, 6 min)	Monocytes	98	16
	T-lymphocytes	92	
Monocyte: B-lymphocytes (20–40 kHz, 10 min: 5 kHz, 6 min)	Monocytes	94	16
	B-lymphocytes	92	
Granulocytes: T-lymphocytes (40–50 kHz, 8 min: 5 kHz, 5 min)	Granulocytes	94	13
	T-lymphocytes	87	
Monocytes: Granulocytes (30–35 kHz, 8 min: 5 kHz, 5 min)	Monocytes	97	13
	Granulocytes	91	

(Adapted with permission from Duhr et al. [63]. Copyright (2000) Biophysical Society).
The DEP field consists of a swept frequency followed by a fixed frequency

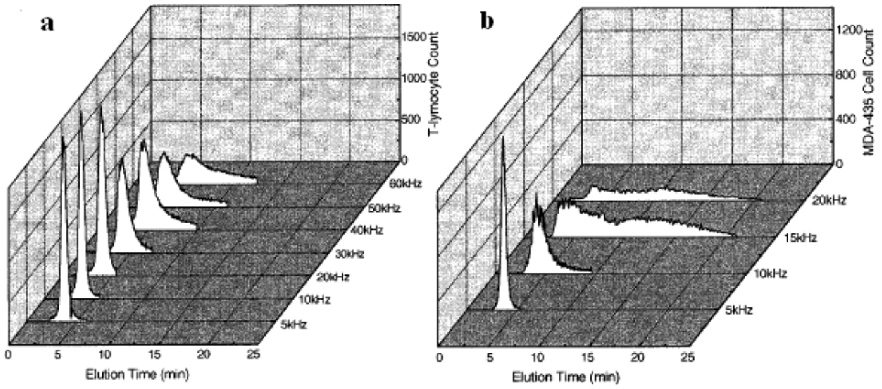

Fig. 15. Frequency-dependence of DiFFF elution profile for (**a**) T-lymphocytes and (**b**) human breast cancer MDA-435 cells. Rapid band broadening of elution fractograms for MDA-435 cells is clearly visible above 10 kHz. Isotonic sucrose/dextrose buffer was used as carrier with 4 V peak to peak DEP field. Reprinted with permission from Wang et al. [58]. Copyright (2000) American Chemical Society

An important FFF related observation made using the DiFFF systems was that the hydrodynamic lift effect was relatively small compared to conventional gravitational FFF systems. Cell elution times were found to be inversely proportional to the flowrate indicating insensitivity of cell equilibrium heights to flow rate. The reason for this result is that hydrodynamic lift forces are very weak (less than 2%) in comparison to the DEP fields [57].

DiFFF is one of the most successful subtypes of microscale FFF and has the potential to be a very important diagnostic tool in cell separation and cancer research. With the ability to sort thousands of cells per minute, DiFFF can be used in conventional labs for sample preparation and other analyses.

7. Microscale Thermal FFF

Thermal field-flow fractionation (ThFFF), one of the oldest FFF subtypes, has primary application in the separation and analysis of dissolved and suspended polymer samples. ThFFF utilizes a temperature gradient across the channel walls to induce separation based on a particle's thermal diffusion coefficient. Thermophoresis in liquid solutions is not well understood and a comprehensive model to predict thermal diffusion of polymers is not

available [64]. ThFFF is similar to ElFFF in that the gradient of temperature generates the field, just as the gradient of voltage generates retention in electrical FFF. To generate the temperature gradient, thermally conductive channel walls are maintained at different temperatures. Polymers typically migrate towards the cold wall under the influence of thermal diffusion and accumulate at the cold wall in what is thought to be an entropic process [65]. A balance between transport and normal-diffusion determines particle retention. A range of solvents such as methanol, THF, acetonitrile, DMSO, toluene, and aqueous solutions with different types of detergents have been employed as carriers in ThFFF.

Applications of ThFFF include the following: molecular weight and size distribution determination, particle size measurement, thermal diffusion coefficient measurements, physiochemical and surface property studies, and separation of particle colloidal mixtures.

Retention in ThFFF system depends on the Soret coefficient, a ratio of thermal diffusion and Fickian diffusion coefficients. The retention parameter can be related to these sample physiochemical properties by

$$\lambda = \frac{D}{\left(D_{\mathrm{T}}\Delta T\right)} = \frac{\kappa T}{3\pi\eta}\left[\frac{10\pi N_A}{3[\eta]MW}\right]^{1/3}\frac{1}{\left(D_{\mathrm{T}}\Delta T\right)}, \tag{37}$$

where, D_{T} is the thermal diffusion coefficient, ΔT is the temperature drop across the channel height, κ is the Boltzmann's constant, T is the average temperature, η is the average carrier viscosity, N_{A} is the Avogadro's constant, $[\eta]$ is the intrinsic viscosity of the dissolved sample, and MW is the average molecular weight of a dissolved sample.

The first successful microfabricated ThFFF system was demonstrated by Edwards et al. [66] and was followed by several reports on mesoscale ThFFF with reduced geometrical dimensions [67, 68] and a microfabricated ThFFF without showing any particle separation [69]. The early ThFFF microsystems were fabricated using techniques similar to the μ-ElFFF fabrication (Fig. 6) with a 27 μm channel thickness, 2–4 mm breadth and 4–6 cm length. These microsystems made of silicon and glass with SU-8 to define the channel walls were fabricated using conventional microfabrication techniques. A thin-film titanium heater on silicon or boron-doped silicon heaters were used to generate the hot wall whereas a glass slide was used as the cold or accumulation wall. Results obtained this early microsystem presented showed a poor temperature drop across the channel due to a poor heat transfer setup. Essentially, silicon with its very high thermal conductivity was found to waste a lot of input energy that was transferred to the environment rather than across the channel. In addition, glass has a high heat capacity and acts as an insulator making it difficult to

maintain a good cold wall temperature. The overall result of these efforts was a very low effective temperature drop available for retention and separation. Later communications [70] from our group showed how the efficiency of heat transfer in ThFFF can be improved by just switching the roles of silicon and glass to cold wall and hot wall respectively. Even with a low temperature drop of ~5.3°C, retention ratios of 0.46 and 0.33 for particles of 204 nm and 272 nm were obtained in a clear separation. Power consumption was reduced 300-fold for a one order of magnitude smaller temperature drop generating similar results when compared to a macroscale system.

8. Miniaturized Flow FFF

Flow field-flow fractionation (FlFFF) is an FFF subtype that relies on cross-flow to compress the sample particles towards the accumulation wall. There are a number of variations of this FFF subtype: conventional (symmetrical), asymmetrical, frit inlet and frit outlet, frit inlet asymmetrical, and hollow fiber FlFFF. Asymmetrical channels have come to dominate in the past few years, since they do not require a perpendicularly applied flow, but rely on flow out of one of the channel walls to generate the gradient. Unlike conventional FFF, the width of the channel progressively shrinks for asymmetrical FFF to maintain a constant field gradient along the length of the channel. For frit inlet asymmetrical FlFFF, the sample is hydrodynamically compressed to the accumulation wall using cross-flow of the carrier solution entering through a small inlet frit as shown in Fig. 16.

A mesoscale frit inlet asymmetrical flow FFF system was fabricated using conventional FFF manufacturing technique [71]. This paper characterized a flow FFF system with only the width and length dimensions being reduced three fold. The channel height was kept at 250 μm as in most conventional FFF systems. This reduced volume system was used to separate a mixture of protein standards with size range between 29 and 700 kD. The reduction in channel width and overall channel volume allowed the use of 10 times smaller flowrates and sample injection volumes. The analysis time was reduced by half (~ 20 min) in comparison to a full-size system for comparable resolution.

While the mesoscale system allowed characterization of a smaller flow-FFF system, it will be interesting to test the performance of a true microsystem with channel heights less than 100 μm. Comprehensive experiments will have to be carried out to check if crossflow can generate a high enough field gradient to induce high resolution separations.

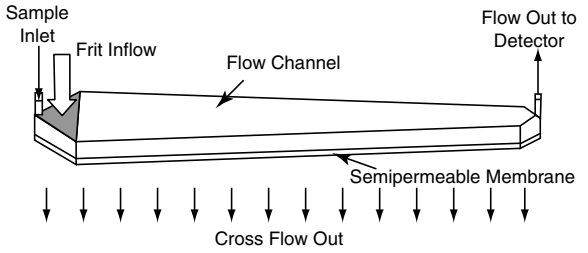

Fig. 16. The asymmetrical-flow field-flow fractionation system with inlet frit and sheet membrane at the accumulation wall

9. Microscale Acoustic FFF

Acoustic/ultrasound-based field-flow fractionation (AcFFF) was first demonstrated by Semenov et al. [72] on the macroscale and fractionation of particles was shown by Beckett's group in several communications for acoustic FFF and SPLITT systems [73–75]. AcFFF is able to separate samples based on density or compressibility of the sample in addition to its size. While most of FFF techniques generate a constant field in the direction normal to the separation direction, the field across the channel varies in AcFFF according to

$$F_{Ac} = \left(-\frac{4}{3}\pi r^3\right) k\overline{E} f(\rho,\gamma) \sin\left(2ky\right), \tag{38}$$

where F_{Ac} is the acoustic force in direction of the field, r is the particle radius, k is the acoustic wave number based on the fundamental wavelength of the acoustic wave, and $\overline{E}$ is the acoustic energy density (function of carrier fluid density and acoustic wave velocity). Equation (38) also indicates a strong dependence of acoustic force on particle size. Factor $f_{(\rho,\gamma)}$ is a function of density and the compressibility of the medium and the particles.

The retention parameter for high retention mode in AcFFF is [76]

$$\lambda = \frac{6\kappa T}{\pi^2 \rho u^2 r^3 \left| f' \right|}, \tag{39}$$

where u is the acoustic wave velocity and $|f'|$ is a function similar to $f_{(\rho,\gamma)}$.

The design of a microsystem with the ability to impart acoustic fields was presented by Edwards et al. [77, 78] and consisted of three layers: an acoustic transducer, a microchannel, and a reflector. Thicknesses for each layer were determined based on the fundamental frequency of the system. Lithium niobate was used as the transducer material and a silicon wafer with input and output ports was used as the reflector plate. A CO_2 laser was used to pattern a thin layer of PDMS, which when sandwiched between the transducer and reflector layers resulted in a μ-AcFFF system [78]. This microsystem showed very poor retention and the retention characteristics did not match with the normal mode or steric mode theory. Nevertheless, it showed a dependence of retention on the applied field and better results were predicted if longer channels were used [78].

10. Other Microscale FFF Efforts

A few other nonconventional FFF techniques have been developed at the microscale, but only a little information has been published on them. For example, the FFF-like SPLITT system, zero-field hydrodynamic chromatography, and a dual field thermal–electrical FFF system have been demonstrated on the microscale. These techniques hold a lot of promise as they expand the FFF applications and provide researchers with more versatile instrumentation.

A microfabricated thermal–electrical system that is capable of imparting both thermal and electrical fields simultaneously using a single instrument was demonstrated on nanoparticles. This system improved retention by 20% with the use of a thermal field (15°C temperature difference) in conjunction with the electrical field [70]. This device design also demonstrated better channel wall material selection can increase the temperature drop across the μ-ThFFF channel.

A technique for minimizing end effects in FFF channels was uniquely demonstrated in a microscale FFF system [79]. For this work, microstructures in the triangular inlet end-pieces were used to distribute sample uniformly across the breadth of the microchannel. A comprehensive fluid flow analysis was used to optimize the size, shape, and locations of the microstructures. Particle dispersion analysis and experimental plate height measurements showed close to a 50% reduction in total plate height for common FFF operating conditions.

10.1. Microscale Split-Flow Thin Fractionation

Split flow thin fractionation (SPLITT) cell is a separation technique very similar to FFF in principle and geometry [80]. Unlike FFF, SPLITT operates continuously and separates the sample stream into two fractions. Since SPLITT can operate continuously, it is ideal for use in applications where high throughput is required.

SPLITT channels have two inlets to introduce the sample and carrier solutions respectively, and two outlets to elute the separated fractions as shown in Fig. 17. The inlet flow splitter prevents unwanted mixing of the two inlet streams and forces the sample input line into a thin stream along one wall of the channel and thus forming the inlet splitting plane (ISP). The applied field perpendicular to the flow of the solution forces susceptible particles across the ISP towards the opposite wall, inducing a binary separation based on the particles' susceptibility to the applied field. The system in Fig. 17 is an example of transport mode SPLITT where the higher transport rates of the black particles allows them to cross the ISP and elute through the lower outlet. For those familiar with microfluidics, this system is similar to the H-filter in principle [81], but adds an external field instead of a concentration gradient as the driving force, which gives SPLITT the possibility of high power separations with higher resolution.

The inherent capability of the system to divide a sample based on a property of the sample particles provides the impetus for sequential or serial separation to yield high volume separation of a complex multicomponent sample. As a first step towards achieving this goal, a microfabricated electrical SPLITT system was fabricated and characterized using polystyrene nanoparticles [80]. Micromachining techniques were used to fabricate a 40 μm thick (channel height) and 2 cm long channel on a glass substrate with gold electrodes in a method similar to that for μ-ElFFF. The microchannel was realized using SU-8 and bonded to another glass substrate using UV curable adhesive.

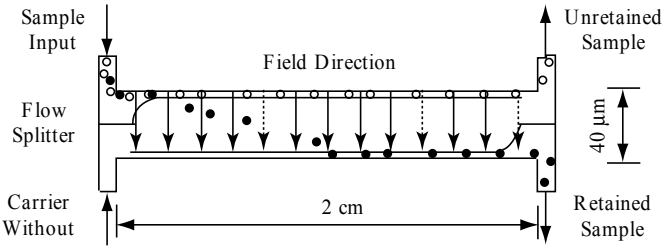

Fig. 17. Schematic diagram of SPLITT system with input and output connections for sample and carrier flow with field direction and illustration of the separation mechanism

Characterization of the system was done using a mixture of 108 nm (μ of 2.47×10^{-4} $cm^2 V^{-1} s^{-1}$) and 220 nm (μ of 4.48×10^{-4} $cm^2 V^{-1} s^{-1}$) diameter polystyrene particles with amine surface groups. SEM images of the eluted particles showed 94% 220 nm particles in one outlet and 70% 108 nm particles in other outlet, a high number selectivity separation at only 1.2 V across the channel. A logical solution to improve the resolution of 108 nm particle sample would be to pass it through another SPLITT channel and adjust the voltage to further separate out 220 nm particles from this stream.

The microfabricated electrical SPLITT system showed potential as a powerful separation technique even with only a 1% effective field due to double layer effects. Serial and parallel combinations of SPLITT channels should result in high resolution and high throughput separations of nanoparticles. In electrical SPLITT system it is relatively easy to control the electrical field in designated areas when compared to thermal or magnetic systems. The ability to program each electrical SPLITT channel separately should result in a tunable resolution and should increase the robustness of the system. There is still significant room for determining optimized channel dimensions for a variety of sample sizes and types in microscale electrical SPLITT channels.

10.2. Microscale Hydrodynamic Chromatography

Hydrodynamic chromatography (HDC) is similar to FFF and is carried out in a channel identical to that used in FFF, but no field is applied. The channel thickness is comparable to the analyte size. A particle size based separation is induced due to the exclusion of particles from areas near the channel walls, just as in steric mode separations in FFF. Larger analytes experience higher velocity flow lines compared to the smaller analytes that can move closer to the wall where flow velocity is a minimum. Figure 18 shows how particles in a hydrodynamic chromatography channel are limited in their motion.

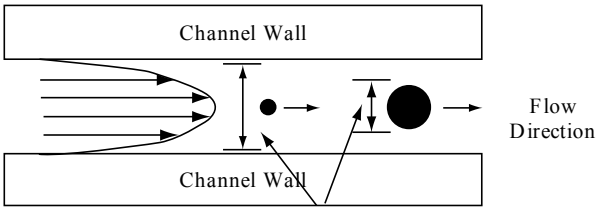

Fig. 18. Hydrodynamic chromatography channel showing the parabolic velocity profile and the regions where a particle can be located

Retention in hydrodynamic chromatography is discussed in several papers [82, 83]. A simple relation between residence time and analyte size is

$$\tau = (1 + B\lambda - C\lambda^2)^{-1}, \tag{40}$$

where τ is the retention time and λ is the nondimensional size of the sample with respect to channel height. B and C are geometry-dependent constants. Several correction factors have been suggested to this basic theory to accommodate for effects such as hydrodynamic interactions with the wall, high velocity-induced inertia effects, and electrostatic or electrokinetic lift forces.

Channel dimensions are predominantly determined by the size of the sample being analyzed. For efficient separation, the channel height should be comparable to the analyte size thus restricting the geometrical dimensions of the HDC channel. This requires thin channels to interrogate smaller samples as is shown in a demonstration of on-chip HDC.

Silicon micromachining was used to realize 1 μm deep, 1,000 μm wide and 8 cm long channels in a 100 mm Si wafer with a 1 μm thick, thermally grown silicon dioxide. Fusion bonding was used to bond the silicon surface with polished Pyrex glass to enclose the channels. Anodic bonding of a Kovar piece with soldered HPLC tubing was used to connect to the input and output ports obtained by powder blasting through the Pyrex. The very small channel volume required on-chip sample injection and UV detection to prevent any extracolumn band broadening that otherwise would have severely affected the separation efficiency.

The distinct separation of particle plugs can be seen in Fig. 19 as the sample travels along the length of the channel [83]. A narrower channel results in better resolution for the smaller sized nanoparticles, likely since band broadening can be associated with the transition from a point injection to a wide channel. Other work showed the separation of proteins and dextran to show biomedical applications of the HDC chip [82].

It is clear that HDC is capable of inducing separation at microscale dimensions without the presence of any external field. Since there is no reliance on an external field, this technique is insensitive to any physiochemical property of the sample and a purely size-based separation can be achieved. Thus, analysis of different sample types using the same instrument should be feasible. Drawbacks of this technique include the requirement for a long separation channel and the limited particle size range that can be separated by a given channel. In addition, a mixture of particles a large size range will result in poor resolution for the smaller particles if the channel is designed to match the larger particles.

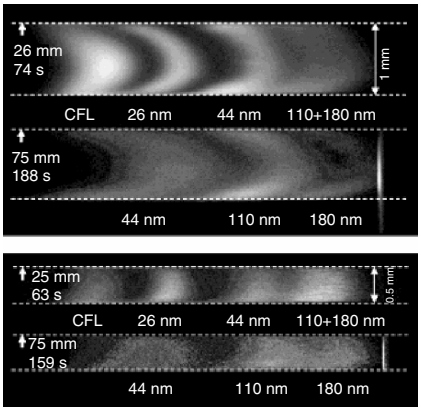

Fig. 19. Top view of the HDC separation of polystyrene nanoparticles and fluorescent marker in different sized microchannels in a silicon-pyrex chip. Reprinted with permission from Blom et al. [83]. Copyright (2003) American Chemical Society

11. Nanoscale FFF

With the recent emphasis on nanotechnology and the development of techniques for nanoscale manufacturing, the question of how FFF might scale to nanometer dimensions comes up. A few researchers have already begun to answer this question, but the fields applied in these systems are usually self generating and not applied externally. Also, electroosmotic flow, instead of pressure-driven flow, tends to be used at nanoscale dimensions, which changes some of the physical processes generating separation.

In a typical electrokinetic separation, such as capillary electrophoresis, the electric field is applied in the direction of the separation in a channel with a significant surface charge on the walls and without any pressure-driven flow. When the dimensions of a channel become comparable to the thickness of the electrical double layer, a particle is subjected to a transverse electrostatic field and a nonuniform flow profile when compared to the plug flow typically associated with electro-osmotic flow. This setup in a nanoscale electrokinetic channel rapidly begins to approach that in a typical FFF channel. Because of the surface charge on the walls, the electrical double layer spreads across the entire height of the electrokinetic nanochannel with most cations approaching the negatively charged glass walls and anions overlapping in the middle of the channel. This charge distribution across the height of the nanochannel results in nonuniform (approaching parabolic) flow

velocity distribution while also exerting a lateral electro-migrative force on the sample. Particles in the channel will be distributed by physics similar to those in normal electrical FFF. The axial migration of the sample is assisted by the main potential gradient along the length of the channel. The main advantages of nanoscale channels over normal electrical FFF is the smaller zone broadening and the ability to operate with high ionic strength carriers. These nanochannels also have the same charge on every wall and so the gradient is between the walls and the center of the channel rather than between the two walls. Thus, every wall could be considered an accumulation wall.

Figure 20 shows images of experimental results showing the separation of fluorescein and bodipy molecules with valence charge (z_s) of –2 and –1 respectively. The FFF-like separation mechanism can be observed as the charge difference of the species results in a distinct retardation in the electromigration of the particles. One important fact to be noticed is the better separation in case of 2-μm deep channel than a 40 nm channel [84, 85]. Extensive numerical modeling of FFF in these types of nanochannels has also been performed [86].

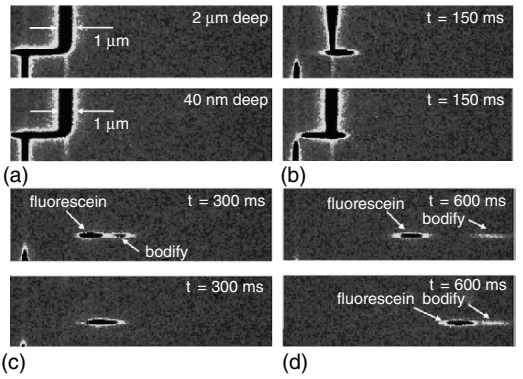

Fig. 20. Separation of fluorescein (z_s = –2) and bodipy (z_s= –1) in channels with depths of 2 μm and 40 nm. The top image in each pair is for a channel of 1 μm width × 2 μm depth with an average liquid velocity of 25 μm s^{-1}. The bottom image in each pair is for a channel of 1 μm width × 40 nm depth with an average liquid velocity of 25 μm s^{-1}. Images are taken at (**a**) injection (time, t=0), (**b**) t=150 ms, (**c**) t=300 ms and (**d**) t=600 ms. Reprinted with permission from pennathur and Santiago [85]. Copyright (2005) American Chemical Society

12. Conclusion

Microscale FFF has shown significant progress since it was first published in early 1997 [87]. Various microscale FFF systems have been used to analyze nanoparticles, DNA, proteins, cells, viruses, polymers, and other materials. A summary of applications is provided in Table 3. Several research groups are now actively exploring applications for these technologies. Since many formats of FFF show significant scaling advantages, there is an opportunity for improvement in these technologies as they are miniaturized. With the advent of the first nanoscale systems, the final potential of these systems is just becoming evident. These FFF channels have also been integrated into more complex analysis systems, and have the potential to be integral components of a lab-on-a-chip system because of their simple operation and easy tuning for specific applications. There are also opportunities to investigate subtechniques in microscale FFF such as magnetic, flow, or sedimentation FFF, which have not yet been explored.

Table 3. Summary table for microscale field-flow fractionation systems

FFF subtype	Physiochemical properties	Applications
Electrical	Size, electrophoretic mobility	Cells and organelles, bacteria and viral separations, characterization of emulsions, liposomes, protein adsorption
Thermal	Size, thermal diffusion coefficient	Separation of dissolved and suspended polymers, polymer and silica nanoparticle analysis
Cyclical electrical	Electrophoretic mobility	Biopolymer separations and zeta potential measurements
Dielectrophoresis	Dielectric permittivity, size	Cell Separation and dielectric property measurements and cancer cell separation
Electrical SPLITT	Size, electrophoretic mobility	High-throughput nanoparticle purification, proteins and starch, clay, viruses, spores, bacteria
Asymmetrical flow	Density, size	Proteins, DNA, polymers, cells, micro and nanoparticles
Hydrodynamic chromatography	Size	Large macromolecule without any charge requirement
Acoustic	Size, density, or compressibility	Macromolecules and nanoparticle separations

Overall, significant promise has been shown, but substantial work needs to be completed before these techniques will be applied broadly.

Acknowledgements

The authors acknowledge funding from the State of Utah Center of Excellence program for some of this work.

References

1. Dittrich P, Tachikawa K, Manz A (2006) Micro total analysis systems. Latest advancements and trends. Anal. Chem. 78: 3887–3907
2. Wang Y, Choi M, Han J (2004) Two-dimensional protein separation with advanced sample and buffer isolation using microfluidic valves. Anal. Chem. 76: 4426–4431
3. Xiao D, Van Le T, Wirth M (2004) Surface modification of the channels of poly(dimethylsiloxane) microfluidic chips with polyacrylamide for fast electrophoretic separations of proteins. Anal. Chem. 76: 2055–2061
4. Araz M, Lee C, Lal A (2003) Ultrasonic separation in microfluidic capillaries. Proc. IEEE Ultrason. Symp. 1: 1066–1069
5. Harris N, Hill M, Beeby S, Shen Y, White N, Hawkes J, Coakley W (2003) Silicon microfluidic ultrasonic separator. Sens. Actuator. B Chem. 95: 425–434
6. Yang S, Zahn J (2004) Particle separation in microfluidic channels using flow rate control. In Proceedings of the ASME Fluids Engineering Division 2004, 127–132
7. Yamada M, Seki M (2006) Microfluidic particle sorter employing flow splitting and recombining. Anal. Chem. 78: 1357–1362
8. Tessier F, Slater G (2002) Strategies for the separation of polyelectrolytes based on non-linear dynamics and entropic ratchets in a simple microfluidic device Appl. Phys. Mat. Sci. Process. 75: 285–291
9. Han J, Craighead H (2000) From microfluidics to nanofluidics: DNA separation using nanofluidic entropic trap array device. Proc. SPIE 4177: 42–48
10. Skulan A, Barrett L, Singh A, Cummings E, Fiechtner G (2005) Fabrication and analysis of spatially uniform field electrokinetic flow devices: Theory and experiment. Anal. Chem. 77: 6790–6797
11. Bousse L (1999) Electrokinetic microfluidic systems. Proc. SPIE 3875: 2–8
12. Ramsey J, Collins G (2005) Integrated microfluidic device for solid-phase extraction coupled to micellar electrokinetic chromatography separation. Anal. Chem. 77: 6664–6670

13. Wang P, Gao J, Lee C (2002) High-resolution chiral separation using microfluidics-based membrane chromatography J. Chromatogr. A 942: 115–122
14. Inglis D, Riehn R, Austin R, Sturm J (2004) Continuous microfluidic immunomagnetic cell separation. Appl. Phys. Lett. 85: 5093–5095
15. Pekas N, Granger M, Tondra M, Popple A, Porter M (2005) Magnetic particle diverter in an integrated microfluidic format. J. Magn. Magn. Mater. 293: 584–588
16. Buch J, Kimball C, Rosenberger F, Highsmith Jr. W, DeVoe D, Lee C (2004) DNA mutation detection in a polymer microfluidic network using temperature gradient gel electrophoresis. Anal. Chem. 76: 874–881
17. Terray A, Hart S, Kuhn K, Arnold J (2004) Optical chromatography in a PDMS microfluidic environment. Proc. SPIE 5514: 695–703
18. Kanagasabapathi T, Dalton C, Kaler K (2005) An integrated PDMS microfluidic device for dielectrophoretic separation of malignant cells. Proc. 3rd Int. Conf. Microchannels Minichannels PART B: 411–418
19. Li Y, Dalton C, Said H, Kaler K (2005) An integrated microfluidic dielectrophoretic (DEP) cell fractionation system. Proc. 3rd Int. Conf. on Microchannels and Minichannels PART B: 403-410
20. Giddings J (1968) Non-equilibrium theory of field-flow fractionation J. Chem. Phys. 81–85:49
21. Giddings J, Caldwell K (1989) Field-flow fractionation. In Rossiter B, Hamilton J (eds) Physical Methods of Chemistry Vol IIIB. Wiley, New York
22. Schimpf M (2000) Resolution and fractionating power. In Schimpf M, Caldwell K, Giddings J (eds) Field-flow fractionation handbook. Wiley-Interscience, New York
23. Giddings J, Schure M (1987) Theoretical analysis of edge effects in field-flow fractionation. Chem. Eng. Sci. 42: 1471–1479
24. Hovingh M, Thompson G, Giddings J (1970) Column parameters in thermal field-flow fractionation. Anal. Chem. 42: 195–203
25. Tri N, Caldwell K, Beckett R (2000) Development of electrical field-flow fractionation. Anal. Chem. 72:1823–1829
26. Davis J (2000) Band broadening and plate height. In Schimpf M, Caldwell K, Giddings J (eds) Field-Flow fractionation handbook. Wiley-Interscience, New York
27. Giddings J (1968) Nonequilibrium theory of field-flow fractionation. J. Chem. Phys. 49: 81
28. Giddings J (1993) Micro-FFF: Theoretical and practical aspects of reducing the dimensions of field-flow fractionation channels. J. Microcolumn. Sep. 5: 497–503
29. Sant H, Gale B (2006) Geometric scaling effects on instrumental plate height in field-flow fractionation. J. Chromatogr. 1104: 282–290.
30. Gale B, Besser R, Papautsky I, Brazzle J, Frazier A (2000) Packaging of biomedical analysis systems. In Proceedings of the Advanced Technology Workshop (ATW) for MEMS and Microsystem Packaging and Integration, Orlando, FL, November 10–12, 2000

31. Kang D, Moon M (2004) Miniaturization of frit inlet asymmetrical flow field-flow fractionation. Anal. Chem. 76: 3851–3855
32. Gale B (1999) Scaling effects in a microfabricated electrical field-flow fractionation system with integrated detector, Ph.D. Dissertation, University of Utah, Utah
33. Gale B, Caldwell K, Frazier A (1998) A micromachined electrical field-flow fractionation (μ-EFFF) system. IEEE Trans. Biomed. Eng. 45:1459–1469
34. Caldwell K, Gao Y (1993) Electrical field-flow fractionation in particle separation. 1. Monodisperse standards. Anal. Chem. 65: 1784–1772
35. Gale B, Caldwell K, Frazier A (2000) Blood and protein separations using a micromachined electrical field-flow fractionation system. In Proceedings of the MicroTAS 2000, Enschede, Netherlands, 399–402
36. Gale B, Caldwell K, Frazier A (2001) Geometric scaling effects in electrical field-flow fractionation. 1. Theoretical analysis. Anal. Chem. 73: 2345–2352
37. Gale B, Caldwell K, Frazier A (2002) Geometric scaling effects in electrical field-flow fractionation. 2. Experimental results. Anal. Chem. 74: 1024–1030
38. Chen Z, Chauhan A (2005) DNA separations by EFFF in a microchannel. J. Colloid Interface Sci. 285: 834–844
39. Palkar S, Schure M (1997) Mechanistic study of electrical field-flow fractionation. II: The effect of sample conductivity on retention. Anal. Chem. 69: 3230–3238
40. Kantak A, Merugu S, Gale B (2006) Particle size and electric field effects in cyclical electrical field-flow fractionation. Electrophoresis 27: 2833–2843
41. Lao A, Trau D, Hsing I (2002) Miniaturized flow fractionation device assisted by a pulsed electric field for nanoparticle separation. Anal. Chem. 74: 5364–5369
42. Sant H, Gale B (2004) Flexible coupling of a waveguide detector with a microscale field-flow fractionation device. Proc. SPIE 5345: 250–257
43. Bartholomeusz D, Boutte R, Andrade J (2005) Xurography: Rapid prototyping of microstructures using a cutting plotter. JMEMS 14: 1364–1374
44. Bard A, Faulkner L (2001) Electrochemical methods: Fundamentals and applications. Wiley, New York
45. Kantak A, Merugu S, Gale B (2006) Carrier ionic strength effects in cyclical electrical field flow fractionation. Anal. Chem. 78: 2557–2564
46. Gale B, Caldwell K, Frazier A (1998) Electrical conductivity particle detector for use in biological and chemical micro-analysis systems. Proc. SPIE 3515: 230–242
47. Gale B, Frazier A (1999) Electrical impedance spectroscopy particle detector for use in microanalysis systems. Proc. SPIE 3877: 190–201
48. Graff M, Frazier A (2006) Resonance light scattering (RLS) detection of nanoparticle separations in a microelectrical field-flow fractionation system. IEEE Trans. Nanotech. 5: 8–13
49. Giddings, JC (1986) Cyclical field field-flow fractionation: A new method based on transport rates. Anal. Chem. 58: 2052–2056

50. Lee S, Myers M, Beckett R, Giddings J (1988) Experimental observation of steric transition phenomena in sedimentation field-flow fractionation. Anal. Chem. 60: 1129–1135
51. Gale B, Merugu S (2005) Cyclical electrical field flow fractionation. Electrophoresis 26: 1623–1632
52. Kantak A, Merugu S, Gale B (2006) Characterization of a microscale cyclical electrical field flow fractionation system. Lab Chip 6: 645–654
53. Biernacki J, Vyas N (2005) A one-dimensional transient model of electrical field flow fractionation. Electrophoresis 26: 18–27
54. Chen Z, Chauhan A (2005) Separation of charged colloids by a combination of pulsating lateral electric fields and poiseuille flow in a 2D channel J. Colloid Interface Sci. 282: 212–222
55. Peterrson M, Giddings J (1984) Sep. Sci. Technol. 19: 307
56 Lyklema J (1995) Fundamentals of Interface and Colloid Science: Vol. II: Solid-Liquid Interfaces. Academic Press Inc, San Diego
57. Yang J, Huang Y, Wang X, Becker F, Gascoyne P (1999) Cell separation on microfabricated electrodes using dielectrophoretic/gravitational field-flow fractionation. Anal. Chem. 71: 911–918
58. Wang X, Yang J, Huang Y, Vykoukai J, Becker F, Gascoyne P (2000) Cell separation by dielectrophoretic field-flow fractionation. Anal. Chem. 72: 832–839
59. Wang X, Vykoukai J, Becker F, Gascoyne P (1998) Separation of polystyrene microbeads using dielectrophoretic/gravitational field-flow fractionation. Biophys. J. 74: 2689–2701
60. Huang Y, Wang X, Becker F, Gascoyne P (1997) Introducing dielectrophoresis as a new force field for field-flow fractionation. Biophys. J. 73: 1118–1129
61. Wang X, Vykoukal J, Becker F, Gascoyne P (1998) Separation of polystyrene microbeads using dielectrophoretic/gravitational field-flow fractionation. Biophys. J. 74: 2689–2701
62. Becker F, Wang X, Huang Y, Pethig R, Vykoukal J, Gascoyne P (1995) Separation of human breast cancer cells from blood by differential dielectric affinity. Proc. Nat. Acad. Sci. 92: 860–864
63. Yang J, Huang Y, Wang X, Becker F, Gascoyne P (2000) Differential analysis of human leukocytes by dielectrophoretic field-flow fractionation. Biophys. J. 78: 2680–2689
64 Duhr S, Arduini S, Brauna D (2004) Thermophoresis of DNA determined by microfuidic fluorescence. Eur. Phys. J. E 15: 277–286
65 Janca J (1988) Field-flow fractionation: Analysis of macromolecules and particles, Marcel Dekker, New York
66. Edwards T, Gale B, Frazier A (2002) A microfabricated thermal field flow fractionation system. Anal. Chem. 74: 1211–1216
67. Janca J (2002) Micro-channel thermal field-flow fractionation: New challenges in analysis of macromolecules and particles. J. Liq. Chrom. Relat. Techn. 25: 683–704

68. Janca J, Ananieva I, Menshikova A, Evseeva T, Dupak J (2004) Effect of channel width on the retention of colloidal particles in polarization, steric, and focussing micro-thermal field-flow fractionation. J. Chromatogr. A 1046: 167–173
69. Bargiel S, Dziuban J, Gorecka-Drzazga A (2004) A micromachined system for the separation of molecules using thermal field-flow fractionation method. Sensor. Actuator. Phys. 110: 328–335
70. Sant H, Gale B (2001) A microfabricated thermal electric field flow fractionation system. Proc MicroTAS 2001 563–564
71. Kang D, Moon M (2004) Miniaturization of frit inlet asymmetrical flow field-flow fractionation. Anal. Chem. 76: 3851–3855
72. Semenov S, Maslow K (1988) Acoustic field-flow fractionation. J. Chromatogr. 446: 151–156
73. Tri N, Beckett R (1999) Ultrasonic forces for particle separations. In Proceedings of the Eighth International Symposium of Field-Flow Fractionation, Paris, France, September 6–8, 1999
74. Beckett R (2001) The use of acoustic forces of thin channel separations. In Proceedings of the Ninth International Symposium on Field-Flow Fractionation, Golden, CO, June 26–29, 2001
75. Tri N, Beckett R (2001) Acoustic field-flow fractionation for particle separation. In Cazes J (eds) Encyclopedia of Chromatography. Marcel Dekker, New York
76. Martin M, Williams P (1992) Theoretical basis of field-flow fractionation. In Dondi F and Guiochort G (eds.) Theoretical advancement in chromatography and related separation techniques. NATO ASI Series C: Mathematical and Physical Sciences Kluwer, Dordrecht, The Netherlands, 383: 534
77. Edwards T, Frazier B (2004) A micro acoustic field-flow fractionation system (μ-AcFFF) for nano-scale separations. In Proceedings of the MicroTAS 2004
78. Edward T (2005) Microfabricated acoustic and thermal field-flow fractionation systems, Ph.D. Dissertation, Georgia Institute of Technology, May 2005
79. Sant H, Kim J, Gale B (2006) Reduction of end-effect induced zone broadening in field-flow fractionation channels. Anal. Chem. 78: 7978–7985
80. Narayanan N, Saldanha A, Gale B (2005) A microfabricated electrical SPLITT system. Lab Chip 6: 105–114
81. Brody J, Yager P (1997) Diffusion-based extraction in a microfabricated device. Sens. Actuator. Phys. 58: 13–18
82. Chmela E, Tijssen R, Blom M, Gardeniers H, Van den berg A (2002) A chip system for size separation of macromolecules and particles by hydrodynamic chromatography. Anal. Chem. 74: 3470–3475
83. Blom M, Chmela E, Oosterbroek R, Tijssen R, Van den berg A (2003) On-chip hydrodynamic chromatography separation and detection of nanoparticles and biomolecules. Anal. Chem. 75: 6781–6768
84. Pennathur S, Santiago J (2005) Electrokinetic transport in nanochannels. 1. Theory. Anal. Chem. 77: 6772–6781

85. Pennathur S, Santiago J (2005) Electrokinetic transport in nanochannels. 2. Experiments. Anal. Chem. 77: 6778–6789
86. Griffiths SK, Nilson RH (2006) Charged species transport, separation and dispersion in nano-scale channels: Autogenous electric field-flow fractionation. Anal. Chem. 78: 8134–8141
87. Gale B, Frazier A, Caldwell K (1997) A micromachined electrical field-flow fractionation system. In Proceedings of the tenth IEEE International Workshop on Micro Electro Mechanical Systems (MEMS '97), Nagoya, Japan 317–322